

PETROPHYSICAL PROPERTIES OF THE WOODFORD FORMATION IN THE
ARDMORE BASIN IN OKLAHOMA, U.S.A

by

BENJAMIN ELLIOTT RYAN

Presented to the Faculty of the Graduate School of
The University of Texas at Arlington in Partial Fulfillment
of the Requirements
for the Degree of

MASTER OF SCIENCE IN EARTH AND ENVIRONMENTAL SCIENCES

THE UNIVERSITY OF TEXAS AT ARLINGTON

November 2017

Copyright © by Benjamin Elliott Ryan 2017

All Rights Reserved



Acknowledgements

I would like to thank the company for providing me with the samples and related data used to complete this research. The support and assistance provided by Seth Conway, Grace Bastianon, Randy Pharis, Gary Burch and many other employees at the company with whom I interacted, made this process as easy as it could be. I would like to thank DrillingInfo for access to the consolidated data set used in this study and IHS for allowing students at the University of Texas at Arlington to use Petra software licenses.

A special thanks goes out to my advisor Dr. Qinhong Hu for providing me with the guidance and direction throughout this process, as well as my committee members, Dr. John Wickham and Dr. Majie Fan. I would like to thank the University of Texas at Arlington as well as the rest of Dr. Hu's research group for their help as well.

Lastly I would like to thank my parents John and Mary Lou as well as my brothers Walker and Henry for supporting me and constantly directing me back to the ultimate source of inspiration, strength and guidance, my Lord and Savior Jesus Christ.

September 1st, 2017

Abstract

PETRO-PHYSICAL PROPERTIES OF THE WOODFORD FORMATION IN THE ARDMORE BASIN IN OKLAHOMA, U.S.A

Benjamin Elliott Ryan, MS

The University of Texas at Arlington, 2017

Supervising Professor: Qinhong Hu

A prolific source rock in Oklahoma, the Woodford Shale has sourced petroleum reservoirs for millions of years and produced oil and gas since 1939. Not until the shale boom of the early 2000's was the full potential of the Woodford Shale, as a reservoir, realized. The focus of this research is to characterize three (the main ones) of the four petro-physically distinct zones within the Ardmore Woodford Shale in order to investigate the ideal zone for hydrocarbon extraction. The Woodford Shale is composed of tight, organic-rich, interbedded shale and chert beds deposited along a marine slope. Due to its tight nature, petro-physical characteristics such as porosity, permeability and fluid flow behavior are hypothesized to be related to pore-throat distribution on the nano-meter scale. A total of seven samples from two wells, cover three of the four zones within the Woodford Shale. Pore framework and fluid flow were investigated using mercury injection capillary pressure (MICP), contact angle (wettability), and spontaneous imbibition tests. Pyrolysis tests were conducted to analyze thermal maturity and TOC, while X-ray diffraction (XRD) tests provided the samples mineral composition. The samples exhibit mineral compositions of mostly quartz and clays with high wettability and pore connectivity when interacting with a hydrophobic fluid of n-decane. Porosity and

permeability values ranged from 0.5 to 3.1% and 4.4×10^{-7} to 1.5×10^{-5} mD respectively, with the majority of pore throats existing within the 5-50 nm range (likely organic matter hosted and/or intraparticle pores). The MICP-derived porosity and permeability results are compared to these obtained from well logs, and a lack of industry standards for measuring tight shale characteristics from core samples makes consistent and repeatable results challenging. An integrated analysis of MICP, imbibition, wettability, geochemistry, well logs, and production data suggests that zone two within the Woodford Shale is the desirable target for hydrocarbon production.

Table of Contents

Acknowledgements	iii
Abstract	iv
Table of Contents	vi
List of Illustrations	viii
List of Tables	xi
Chapter 1 Introduction.....	1
Chapter 2	4
2-1 Geologic Setting and Depositional Environment.....	4
2-2 Stratigraphy	7
2-3 Well Log Interpretation	9
2-4 Industry Standards for Shale Rock Characterization	14
Chapter 3 Methods.....	17
3-1 Acquisition of Samples	17
3-2 XRD and Geochemistry.....	21
3-3 Wettability and Contact Angle	23
3-4 Mercury Injection Capillary Pressure (MICP)	24
Procedure for MICP Tests	26
3-5 Fluid Imbibition	28
3-6 Log Analysis	30
3-7 Production Data.....	32
Chapter 4 Results	33
4-1 Mineralogy and Geochemistry.....	33
4-2 Wettability	43
4-3 Mercury Injection Capillary Pressure (MICP)	48

4-4 Imbibition	54
4-5 Log Analysis	58
4-6 Porosity and Permeability from Different Approaches	60
4-7 Production Data.....	63
Chapter 5 Discussion.....	66
5-1 Mineralogy and Geochemistry.....	66
5-2 Wettability	69
5-3 Pore Structure Characteristics from MICP Analysis.....	69
5-4 Pore Connectivity	70
5-5 Porosity and Permeability.....	71
5-6 Well Logging and Producibility	73
Chapter 6 Conclusions and Recommendations	74
6-1 Conclusions	74
6-2 Recommendations	75
Appendix A XRD Standard Operating Procedure.....	76
Appendix B TOC Standard Operating Procedure.....	80
References.....	83
Biographical Information	90

List of Illustrations

Figure 1-1 Major US shale plays with Woodford highlighted in bright red (modified from EIA, 2016)	3
Figure 1-2 Location Map of Ardmore Basin and two sample wells (A and E) used in this work (modified from Northcutt and Cambell 1995)	3
Figure 2-1 Paleogeographic maps of Texas, New Mexico, Oklahoma, and Louisiana at (A) 385 Ma, (B) 385 Ma, and (C) 360 Ma (Comer, 2008)	6
Figure 2-2 Woodford Isopach Map in Ardmore Basin (EIA, 2011)	7
Figure 2-3 Ardmore Basin Stratigraphic Column (modified from Blackford, 2007)	9
Figure 2-4 Location Map for the 7 well Cross Section A - A' detailed in Figure 2-5 (DrillingInfo, 2017).....	10
Figure 2-5 Structural Cross Section A - A' (Petra, 2017).....	11
Figure 2-6 A type log at Ardmore Basin.....	12
Figure 2-7 Triple Combo Log Suite for Log A. Samples were taken at depths of 8566' MD (middle depth), 8639' MD, 8722' MD, 8829' MD. WDFD means Woodford.	13
Figure 2-8 Triple Combo Log Suite for Log E. Samples were taken at depths of 6609' MD, 6692' MD, 6829' MD.....	14
Figure 3-1 Photos upon sample arrival: (a) Full sample taken with a digital camera (b) Sample surface taken at x20 zoom (scale bars are present in images at bottom-left corners, and the lamination looking marks in the photos are cutting marks).....	20
Figure 3-2 Example of epoxied cube indicating bottom face (to be in contact with imbibition fluid) and epoxied faces; number 1 indicates cube #1 while H indicates that imbibition direction will occur parallel (horizontal) to the bedding plane.....	21
Figure 3-3 Schematic of the Apparatus for Imbibition Test (Gao & Hu, 2012)	29

Figure 4-1 X-ray Diffraction (XRD) Results for Samples from Well A (A-D) and Well E (E-G)	36
Figure 4-2 Diagram for sCore Lithofacies Classification Scheme for Organic Mudstones for Wells A and E	37
Figure 4-3 S2 vs. TOC, Partitioned by Kerogen Type, and Colored by Laboratory where Results were Collected	39
Figure 4-4 S1 vs TOC with Oil Crossover, Colored by Laboratory Analysis	40
Figure 4-5 Depth vs. TOC (wt%) and S1 (mg HC/g rock), Oil Crossover Shaded in Green, for Well E RTC data	41
Figure 4-6 Contact Angle Measurements a) A8566 b) A8639 c) A8722 d) A8829 e) E6609 f) E6692 g) E6829	46
Figure 4-7 Log differential intrusion vs. intrusion pressure for sample A8829.....	50
Figure 4-8 Graphical representation of pore-throat size distribution from MICP tests	52
Figure 4-9 DI water imbibition into sample E6692 for A) 4 and B) 24 hours	56
Figure 4-10 n-decane imbibition into sample E6829 for 4 hours	57
Figure 4-11 Log Analyses of Well A.....	59
Figure 4-12 Log Analyses of Well E.....	60
Figure 4-13 Porosity cross plot for Well A.....	62
Figure 4-14 Porosity cross plot for Well E.....	62
Figure 4-15 Cumulative Monthly Production over Time for Well A from DrillingInfo (the company declines to provide daily production/pressure data, as well as any operation factors related to production bumps).	64
Figure 4-16 Cumulative Production over Time for Well E.....	65
Figure 5-1 Mineral percentages vs. TOC.....	66
Figure 5-2 Quartz vs. Porosity	68

Figure 5-3 Clay vs. Porosity	68
Figure 5-4 Porosity vs. TOC	72
Figure 5-5 Comparison of Permeability Values from Various Techniques	72

List of Tables

Table 2-1 Data Acquired at RTC.....	16
Table 4-1 Summary of XRD results obtained from Shimadzu Center	37
Table 4-2 Pyrolysis Results	42
Table 4-3 Qualitative Droplet Wettability Result	43
Table 4-4 Droplet Wettability Images.....	44
Table 4-5 Compilation of Contact Angles	47
Table 4-6 Wettability 2 μ L Images	47
Table 4-7 Pore-throat Size Distribution (%); A, B, C denotes replicate analyses.....	49
Table 4-8 Pore characteristics obtained through MICP Analyses	53
Table 4-9 List of Imbibition Tests Performed.....	55
Table 4-10 Region III average slope for imbibition tests.....	57
Table 4-11 Porosity Results from Various Approaches	61
Table 4-12 Permeability Results from Various Approaches	61
Table 4-13 Completion details for study wells	63

Chapter 1

Introduction

The Woodford Shale has historically been considered a mature source rock throughout much of Oklahoma and parts of Texas and New Mexico, and gained reputation as a prolific oil and gas reservoir since the onset of the shale boom in the early 2000's (Figure 1-1). The most widespread Woodford Shale lithology is black shale, and other lithologies include chert, siltstone, sandstone, dolostone, and light colored shale (Comer, 2008). The heterogeneous characteristics of shale reservoirs at the nanometer scale, coupled with processes such as gas desorption, the Klinkenberg effect, and rock deformation, make it difficult to predict production and quantify the economics of tight shale wells. A greater understanding of the relationship between pore structure and fluid flow will lead to better production stimulation techniques (Ding, 2014). In conventional reservoirs, the focus is on draining a field where hydrocarbon flow is relatively unrestricted into the borehole. In unconventional reservoirs the production is very weak without opening fracture networks surrounding the wellbore by the injection of thousands of gallons of water and proppants. The focus then moves from draining a field to draining the immediate shale matrix area surrounding the fracture network. Continued research is necessary for the industry to develop more efficient well placement and hydraulic fracturing designs to realize economic production from unconventional plays in today's low price environment.

It is estimated that the state of Oklahoma, as a whole, has proved crude oil in place of roughly 1,262 million barrels as of 2015 (EIA), but due to well production decline, field production decline, average well quality, and finite number of potential wells, only a small percentage of this reserve number will ever actually be produced. Plays have a finite number of drillable locations, and the "sweet spots" where the production and

economics are the highest are usually drilled early on in the play's lifecycle. These wells still have production decline rates of 75-85% in the first three years while the field production declines by 30-45% per year (Hughes, 2015). In order to keep up with these decline rates, more wells have to be drilled, thus exhausting the finite drilling locations. Ideally these decline rates would be much lower allowing for an efficient and economical drilling program to extract more of the oil in place. Steep production decline could be due to pore structure and fluid flow, petro-physical characteristics that are not well understood in tight shales (Hu et al., 2014).

Covering an 80 km long by 10 km wide area, the Ardmore Basin exists mostly in Carter and Marshall Counties, but extends into the southwest corner of Johnston County as well (Figure 1-2). It was not until 2005 that the Ardmore Woodford Shale play began to gain interest, and from 2005 to 2011, shale wells have produced roughly 662 million cubic feet of gas (MMCF) and 7 thousand barrels of oil (MBO) (Boyd, 2011). It is estimated that the field holds four trillion cubic feet of natural gas (TCF) (Ballotpedia, 2015). Ranging in thickness from 180 to 500 feet and a depth of 6,000 to 12,000 feet, the Woodford unconformity overlies the Hunton. Within the basin, total organic content (TOC) values range from 2-20% with low permeability, while porosity measurements average about 4% (Jarvie, 2008).

The focus of this research is on the nanopetrophysics of the Devonian aged silty black shale and chert located within the Woodford Formation of the Ardmore basin. The purpose is to consider patterns between hydrocarbon storage (pore size distribution, porosity), transport (wettability, permeability, and tortuosity), and production. The measurements of these properties as well as well log analyses will provide valuable insight into the desirable Woodford zone for sustained hydrocarbon production.

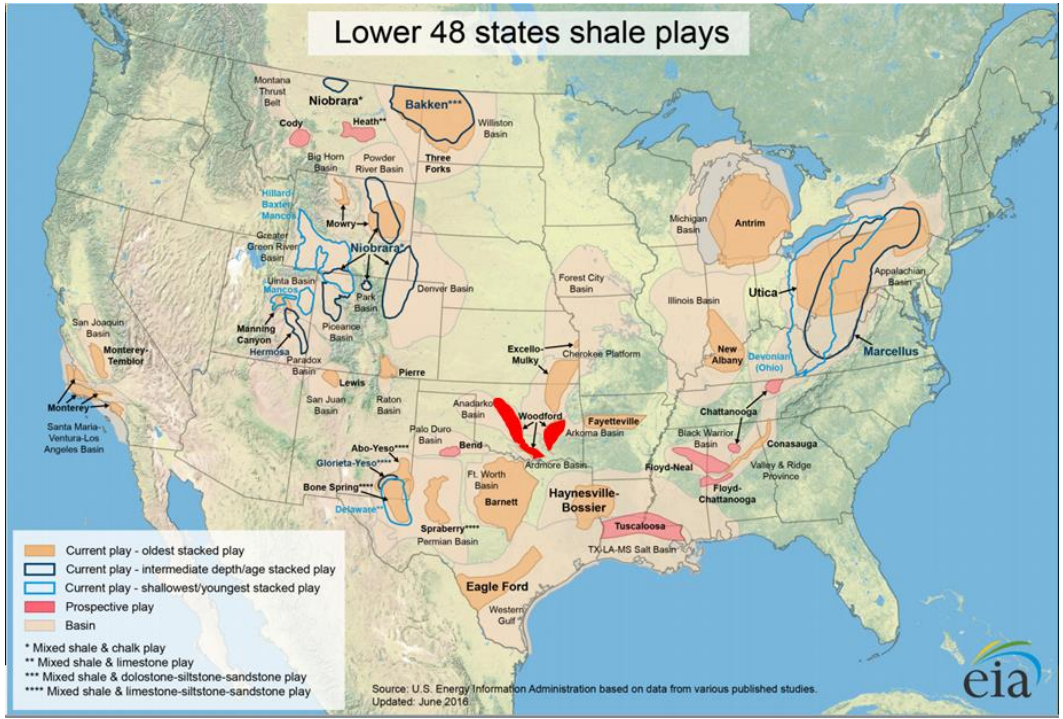


Figure 1-1 Major US shale plays with Woodford highlighted in bright red (modified from EIA, 2016)

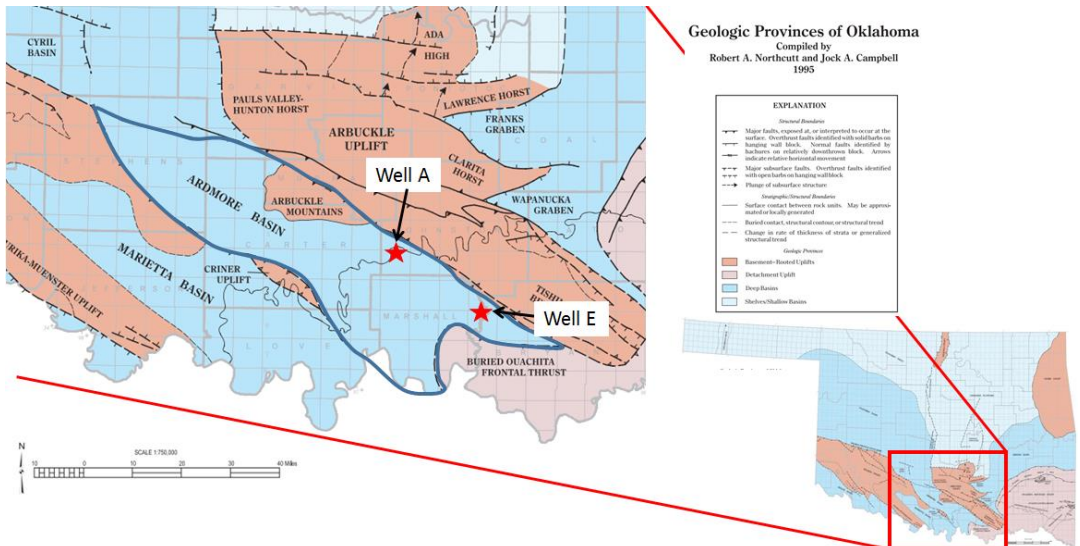


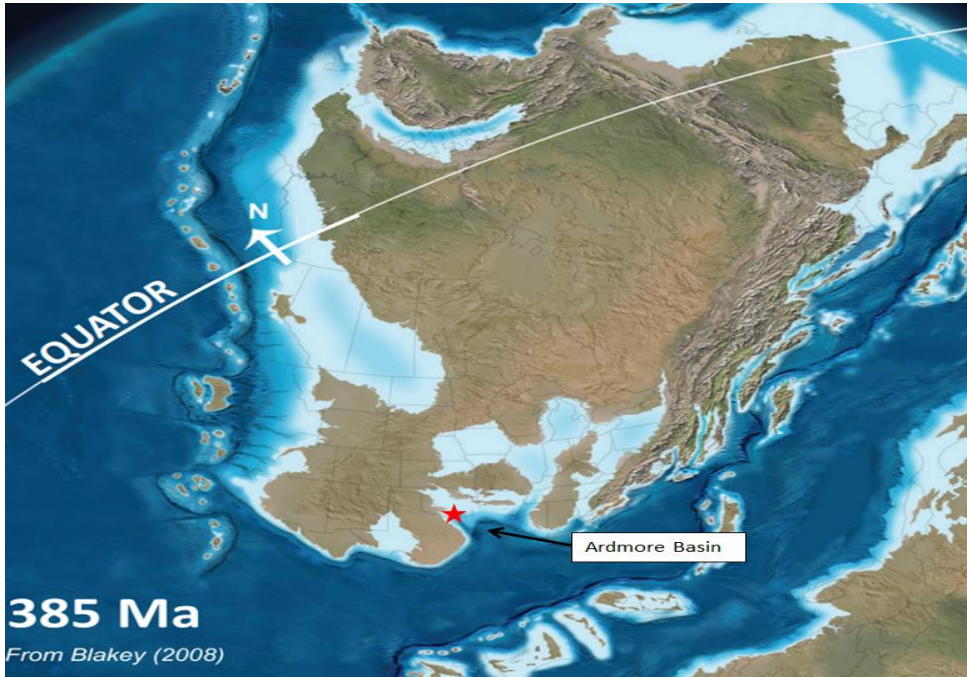
Figure 1-2 Location Map of Ardmore Basin and two sample wells (A and E) used in this work (modified from Northcutt and Campbell 1995)

Chapter 2

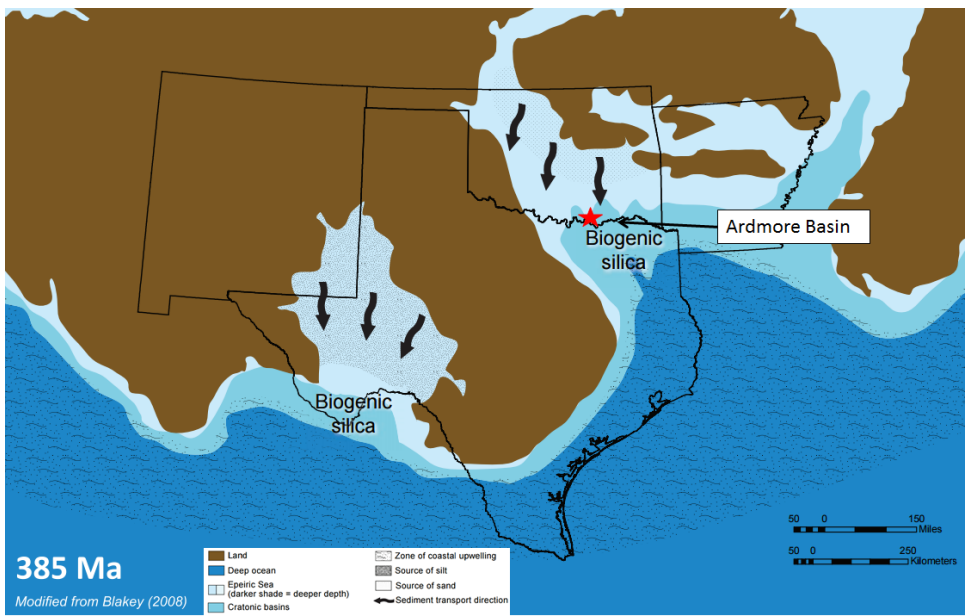
2-1 Geologic Setting and Depositional Environment

This study focuses on the Woodford Shale located along the northeast margin of the Ardmore Basin in south central Oklahoma (Fig. 1-2). Extreme structural deformation has occurred throughout southern Oklahoma, making the geologic history crucial for successful exploration and production. Southern Oklahoma was formed sometime in the Late Proterozoic Eon between 525 and 500 million years ago during the rifting of Laurentia. Two of the three original rift arms became spreading zones for the Iapetus Ocean. According to Pearson (2014), "Subsidence occurred from Late Cambrian through Early Mississippian time, and was dominated by thermally controlled isostatic subsidence caused primarily by cooling of the southern Oklahoma aulacogen". This cooling event created accommodation space in the southern Oklahoma trough, which lined up geometrically with the failed rift arm of the southern Oklahoma aulacogen, allowing nearly 12,000 feet of Cambrian-Devonian sediment to be deposited in a marine environment (Figure 2-1 A). The Woodford Shale was deposited along the continental margin where marine transgression flooded the craton, creating an extensive epeiric sea that covered all but a few isolated areas during eustatic highstand (Comer, 2008). Figure 2-1 A through C below displays paleogeographic maps of North America during the deposition of the Woodford Shale. Beginning in the Pennsylvanian, multiple orogenic events occurred to create the complex structure that defines Oklahoma basins today.

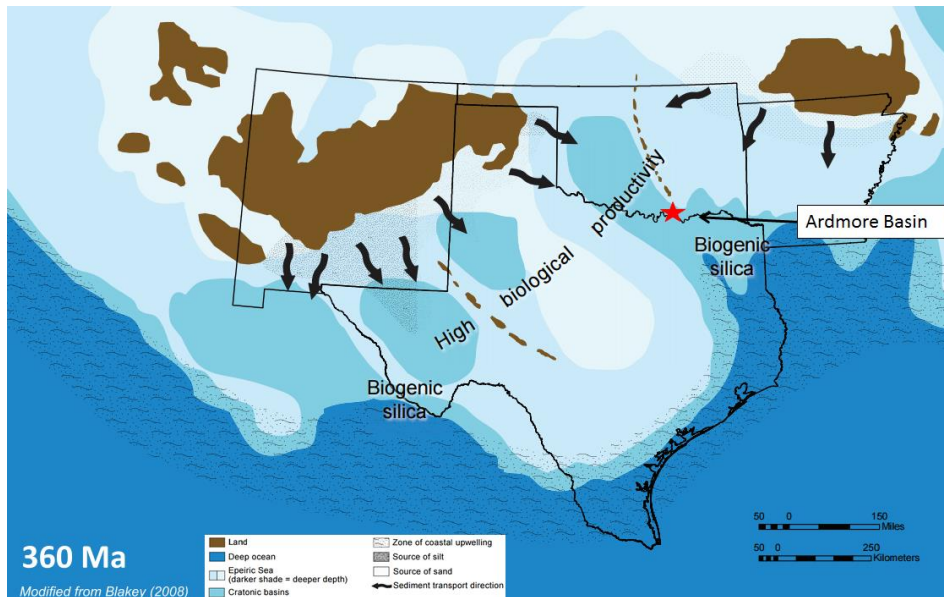
Subsidence and faulting occurred in the Ardmore Basin until the end of the Pennsylvanian (Granath, 1989; Suneson, 1996).



(A)



(B)



(C)

Figure 2-1 Paleogeographic maps of Texas, New Mexico, Oklahoma, and Louisiana at (A) 385 Ma, (B) 385 Ma, and (C) 360 Ma (Comer, 2008)

The Ardmore Basin is bounded to the northeast by the Washita valley fault and Arbuckle Uplift, while to the southwest it is bounded by the Criner Hills Uplift and Marietta Basin. To the northwest is the Anadarko Basin, and to the southeast lies the Ouachita Thrust Belt (Kilic and Tapp, 2014; Allen 2000). Due to the collision of the North and South American plates during the Paleozoic, the basin experienced multidirectional stress fields which created left lateral strike slip structures involving oblique normal, reverse, and thrust faults (Harding, 1974). This caused a regional shortening of the basin by roughly twenty percent creating the current structure visible in Figure 2-2. As sea level rose in the late Devonian, upwelling of biogenic silica-rich oceanic water (shown in Figure 2-1 B and C) maintained a normal marine biota within the shallow water column while net evaporation produced hypersaline brine. The brine developed density currents restricting

vertical mixing in the water column and creating an anoxic environment on the sea floor where pelagic debris settled as organic- and sulfide-rich mud (Comer, 2008). Both the depositional and burial histories of the Woodford Shale provide the perfect scenario for oil and gas generation.

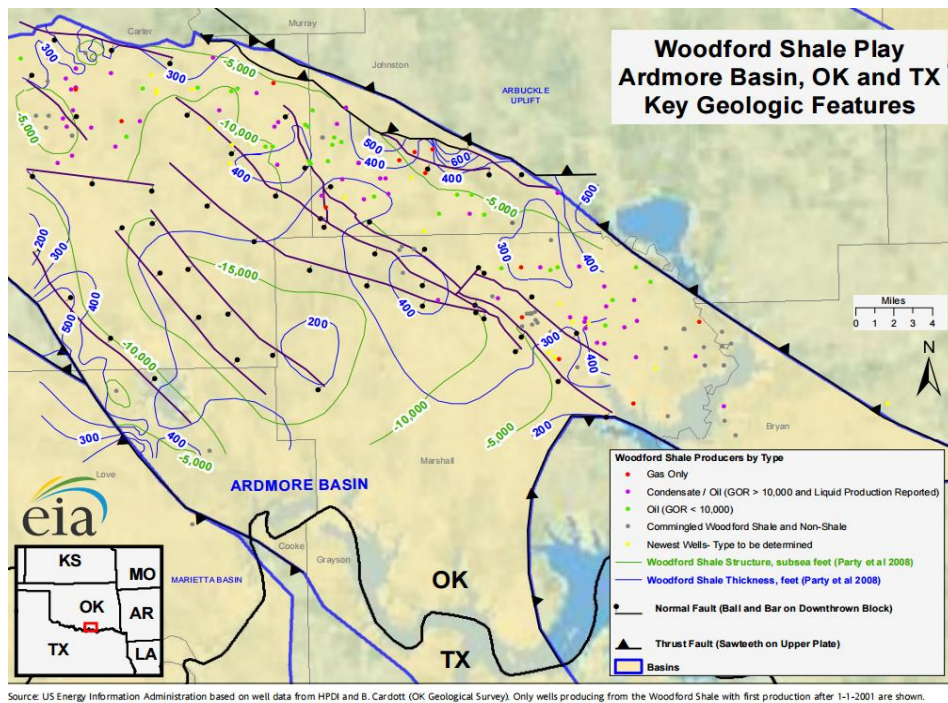


Figure 2-2 Woodford Isopach Map in Ardmore Basin (EIA, 2011)

2-2 Stratigraphy

The Woodford Formation in the Ardmore Basin was deposited during the Middle Devonian to Early Mississippian. It was deposited over a regional unconformity existing in the Hunton group, and is overlain by the Sycamore Limestone as seen on the stratigraphic column in Figure 2-3. The Woodford is a mudrock with finely interbedded and alternating layers of chert, siliceous shales, siltstone, sandstone, and dolostone

(Fertl, Chilingarian 1990). The beds are mostly dark brown to black when cored, but have a tan color after being exposed and weathered at the surface. The formation ranges in thickness from 180-500 feet. Up until recently three zones (1, 2, and 3) have been used to describe the Woodford throughout Oklahoma and Texas, but based on petrophysical correlations the third zone can be further divided into two zones creating four zones in total. The fourth zone exists where there is enough accommodation space for a deep water mudstone to have been deposited during the Middle Devonian. It is missing to the northwest and southeast, due to an uplift and erosion caused by the Arbuckle Orogeny. These four units shown below are identified primarily based on the gamma ray signature to indicate marine transgression and regression (Slatt, 2013):

Zone 1 is the youngest zone in the Woodford which was deposited at the end of the Devonian. It consists of interbedded chert and black shale beds with parallel laminae, exhibiting low gamma ray and resistivity signatures. This zone thins upwards towards the Sycamore formation (Comer, 2008; Blackford, 2007).

Zone 2 produces a high gamma ray response and contains shales, siltstones, dolostones, chert beds as well as phosphatic nodules. The beds contain parallel laminae, high concentrations of organic carbon, conodonts and many resinous pores (Comer, 2008).

Zone 3 contains more carbonate, silt, and sand than the other zones, and overlies the regional unconformity when the fourth zone is absent. It contains no phosphate nodules and produces a large range of gamma ray and resistivity signatures (Slatt, 2015).

Zone 4 is the oldest zone deposited onto the regional unconformity above the Hunton group (Figure 2-3). It is primarily dominated by mudstone and characterized by extremely low gamma ray and resistivity signatures.

Historically the best unconventional wells have been completed in the naturally fractured, thermally mature, organic-rich, cherty facies of the Woodford Shale, which place significant importance on Zones 1 and 2 (Burch, 2016). Targeting these zones might provide a greater rate of penetration while drilling, as compared to the mudstone in Zone 4.

Eon	Era	Period	Formation		Unit		
PHANEROZOIC	PALEOZOIC	MISSISSIPPIAN	E	Sycamore			
			L	WOODFORD	Zone 1		
		Zone 2					
		Zone 3					
		Zone 4					
		DEVONIAN	HUNTON	M			
				E			
				L	SILURIAN	L	
						M	
						E	

Figure 2-3 Ardmore Basin Stratigraphic Column (modified from Blackford, 2007)

2-3 Well Log Interpretation

According to Drilling Info (2017), there have been roughly 500,000 wells drilled in Oklahoma. It is possible to thoroughly map subsurface geology throughout southern Oklahoma from the digital and raster logs acquired during the drilling of these wells. A

SW-NE structural cross section of seven wells presents the dip profile of the Ardmore Basin (Figs. 2-4 and 2-5). The Woodford to the northeast encounters shallower depths and liquid-rich gas production. This structure is the focus of drilling in the basin, apparent by the greater concentration of wells shown in blue in Figure 2-4. To the southwest, the Woodford drops off to reach approximate depths of 19,000'. There is a low concentration of wells here due to the production difficulties and the existence of over-mature hydrocarbons encountered at this depth. In Figure 2-5, the prevalent formations, Primrose, Caney, Woodford, and Viola, are marked to aid in the visualization of the basin structure.

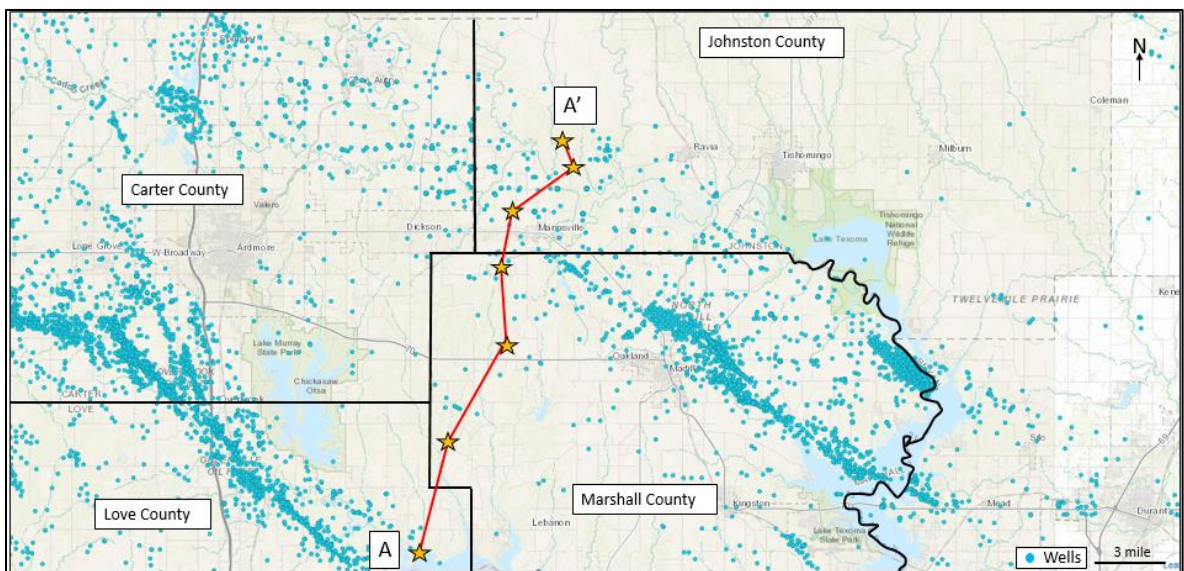


Figure 2-4 Location Map for the 7 well Cross Section A - A' detailed in Figure 2-5 (DrillingInfo, 2017)

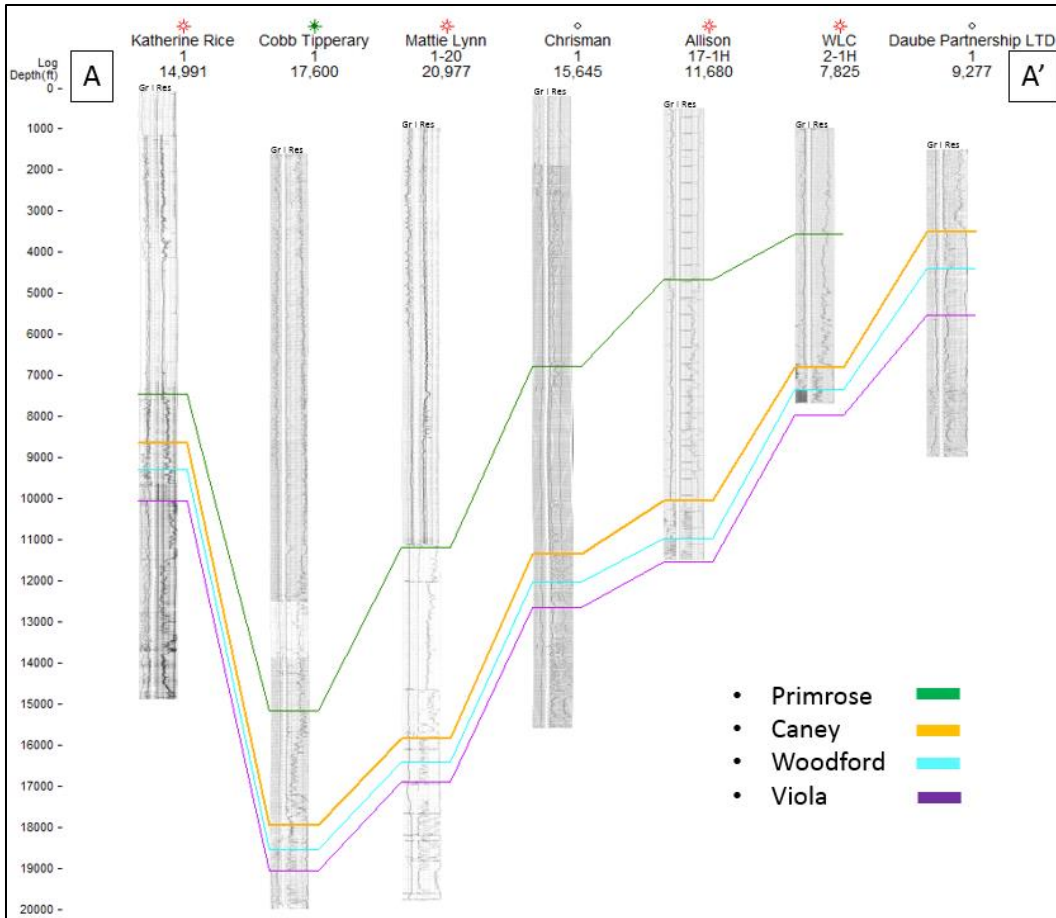


Figure 2-5 Structural Cross Section A - A' (Petra, 2017)

Digital logs provide valuable insight into the rock properties of the Woodford Shale, and allow for samples to be carefully picked within the different lithological zones for laboratory studies. In this work, further calculations are performed using these logs in order to derive porosity and permeability values. When correlating and mapping within a basin, it is important to locate a type log well, an ideal representation of the local stratigraphic section. This well should present the formations without missing sections and at original depositional thicknesses. **Figure 2-6** below shows a type log for the Ardmore Basin, where the Caney, Woodford, and top of the Hunton/Sylvan formation are

shown. The Woodford is roughly 340 feet thick, with relatively high gamma ray values indicating a shaly lithology. Sitting on top of the Woodford, the Sycamore is approximately 360 feet thick and contains carbonates, sandstones, and limestones. Furthermore, the Caney sits on top of the Sycamore at approximately 400 feet thick containing carbonates and shales (Fig 2-6).

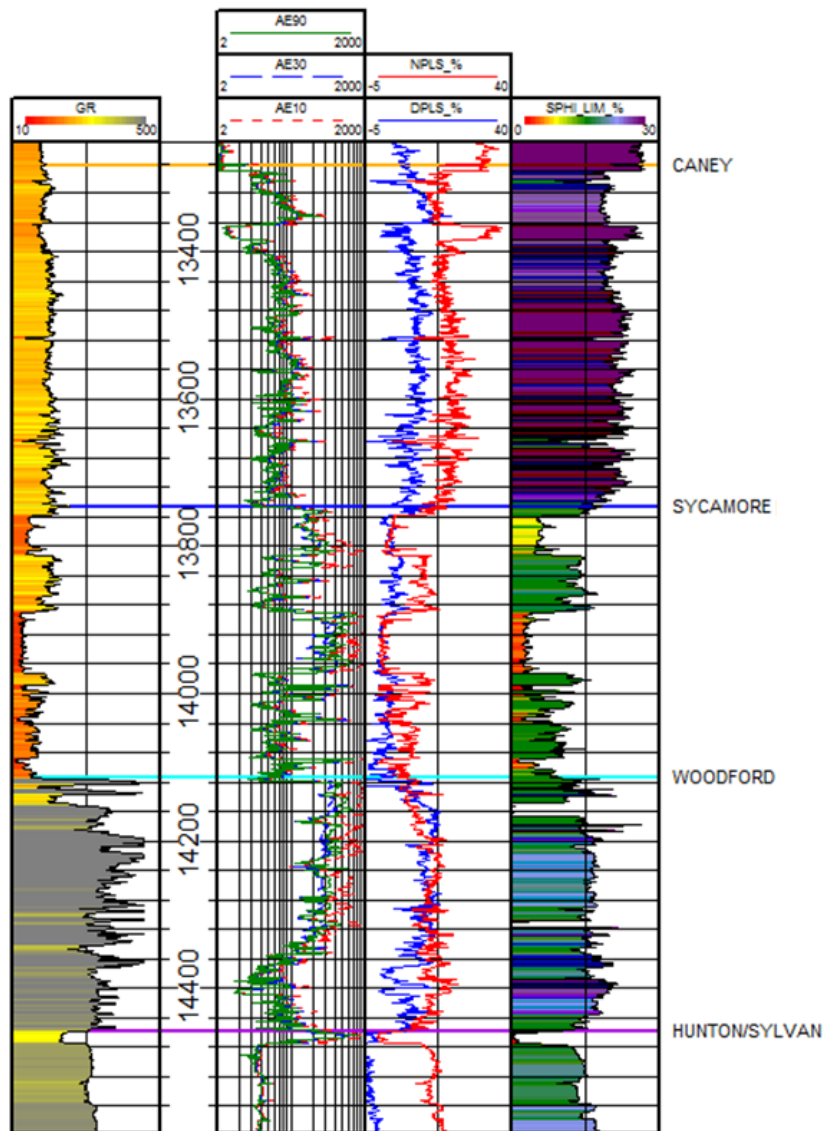


Figure 2-6 A type log at Ardmore Basin

A traditional triple combo log suite is presented below in Figures 2-7 and 2-8 for Wells A and E, respectively. The depths of the four Woodford zones and locations of the core samples chosen for this study are identified on each well.

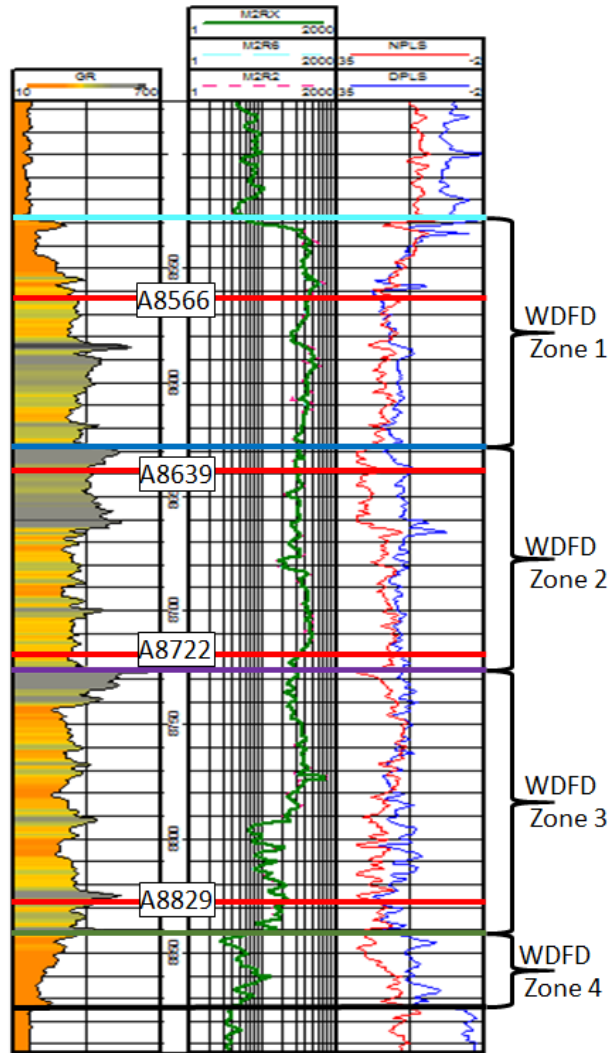


Figure 2-7 Triple Combo Log Suite for Log A. Samples were taken at depths of 8566' MD (middle depth), 8639' MD, 8722' MD, 8829' MD. WDFD means Woodford.

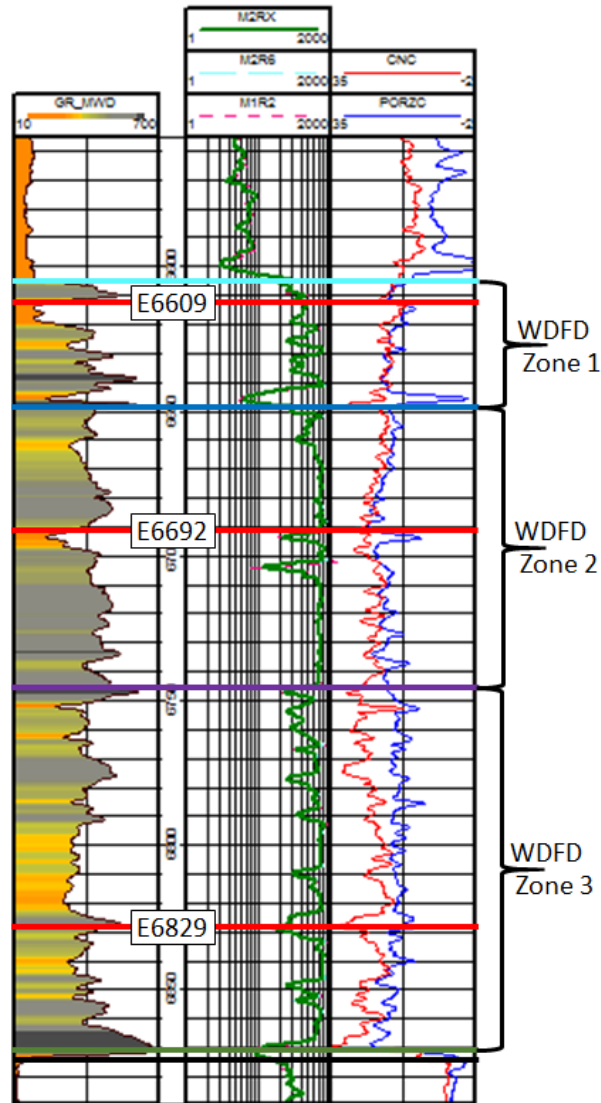


Figure 2-8 Triple Combo Log Suite for Log E. Samples were taken at depths of 6609' MD, 6692' MD, 6829' MD

2-4 Industry Standards for Shale Rock Characterization

The techniques and methods used in core analysis facilities to measure the basic rock properties (e.g. porosity and permeability values) have changed rapidly with the rise of shale plays in the United States. The focus is now on extracting fluids from a pore-

network that is on the nanometer, rather than the micrometer, scales, which presents unique measurement challenges. There are various core analysis protocols being used in different laboratories, leading to inconsistent measurements, even when measuring on similar sample sets taken from the same depths (Sondergeld, 2010). This provides a confusing picture for an operating company without its own core lab, who might use different laboratories over time which is based on the fluctuating price of service. The same phenomenon can be seen within the research industry where different laboratories are not producing the same results when analyzing the same shale rock. In order to cut through some of the confusion and better understand shale rock, an industry standard test suite must be developed (Sondergeld, 2010). The samples used for this research were analyzed by the Reservoir Technology Center (RTC) at Chesapeake Energy and the data is shown below in Table 2-1. These results will be compared with new results collected in this thesis to comment on the consistency between shale rock property measurements from different laboratories, with respect to density, porosity, and permeability.

Table 2-1 Data Acquired at RTC

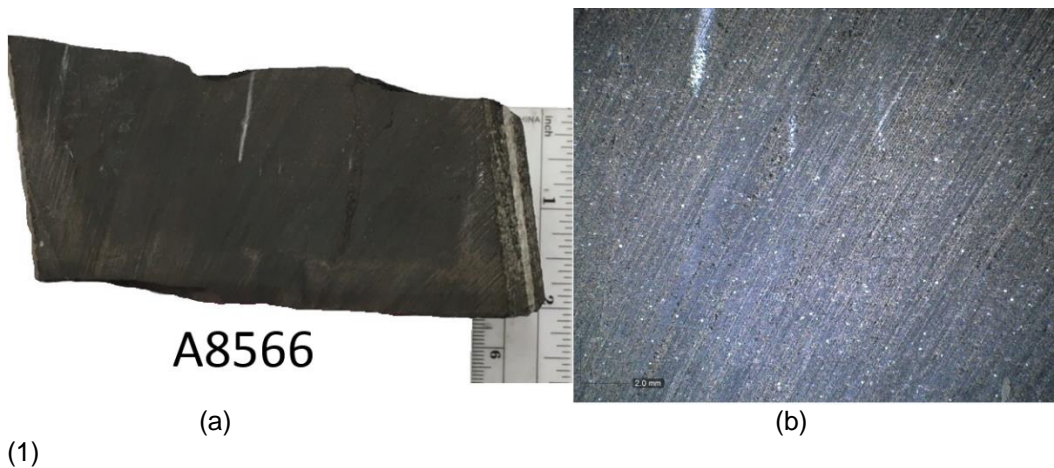
	A8566	A8639	A8722	A8829	E6609	E6692	E6829
A-R Bulk Density (g/cm³)	2.56	2.35	2.35	2.11	2.3	2.29	2.32
A-R Grain Density (g/cm³)	2.65	2.4	2.43	2.16	2.37	2.34	2.35
A-R-Minus Oil Grain Density (g/cm³)	2.72	2.46	2.51	2.22	2.38	2.34	2.37
Dry Gain Density (g/cm³)	2.75	2.48	2.54	2.24	2.39	2.35	2.7
Porosity (% of BV)	7.91	6.61	9.39	7.22	4.17	3.27	2.71
Water Saturation (% of PV)	6.59	6.03	4.24	4.96	12.8	4.92	8.93
Gas Saturation (% of PV)	40.7	30	35.6	31.6	71.9	63.6	50.4
Mobile Oil Saturation (% of PV)	52.7	63.9	60.1	63.5	15.3	31.5	40.6
Gas Filled Porosity (% of BV)	3.22	1.99	3.35	2.28	3	2.08	1.37
Expandable Clay Water (% of BV)	4.24	3.79	5.03	4.23	1.02	0.28	0.37
Bound Hydrocarbon Saturation (% of BV)	7.63	4.01	5.28	8.58	7.55	6.57	6.29
Bound Clay Water (% of BV)	2.95	3.59	1.99	1.08	4.67	3.15	4.38
12-20 Mesh Permeability (mD)	1.42x10 ⁻⁴	1.59x10 ⁻⁴	2.38x10 ⁻⁴	1.32x10 ⁻⁴	NA	NA	NA
6-12 Mesh Permeability (mD)	9.94x10 ⁻⁴	2.64x10 ⁻³	8.14x10 ⁻⁴	7.74x10 ⁻⁴	NA	NA	NA
CO₂/Toluene GRI Mesh Permeability (mD)	NA	NA	NA	NA	4.77x10 ⁻⁴	1.09x10 ⁻³	7.17x10 ⁻⁴

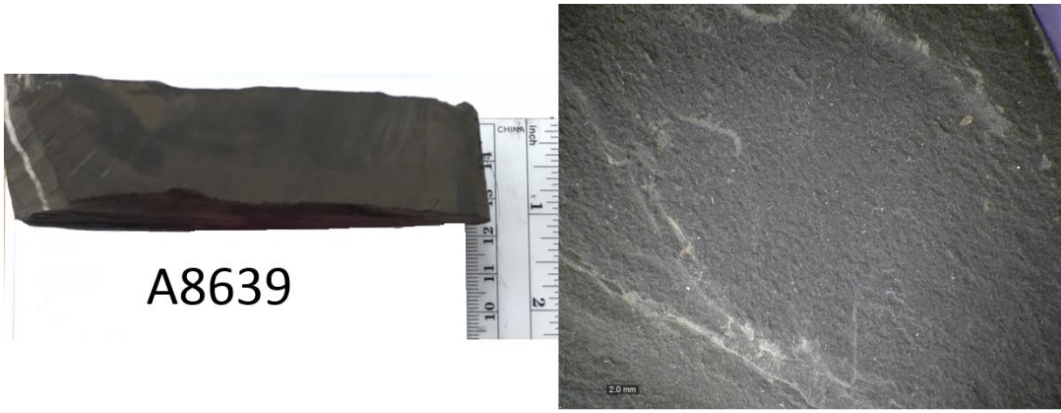
Note: A-R: as received; PV: pore volume; BV: bulk volume; mD: millidarcy.

Chapter 3 Methods

3-1 Acquisition of Samples

Core samples, pyrolysis, XRD, and measured rock characteristics such as liquid saturation, permeability, and bulk density were provided by the company for two wells (A and E) within the Ardmore Basin (Table 2-1). The wells are located roughly 30 miles apart. Approximately 440' of Well A and 425' of Well E were cored. Multiple trips were made to the company's core facility to select and package the core samples to be used in this study. The larger slab from Well A was examined and samples were taken at depths of 8566', 8639', 8722', and 8829', representing the top three of the four petro-physically distinct zones. In Well E, large slab samples were taken from the top three Woodford Zones (1 to 3) at depths of 6609', 6692', and 6829'; Zone 4 is nonexistent in Well E. Sample photos were taken with both digital and microscopic cameras shown in Figure 3-1 1 through 7; note that lighting conditions are not consistent throughout so colors are not comparable. Photo series A was taken with a digital camera in order to include the whole sample (> 4 cm across), while photo series B was taken at x20 zoom with a microscopic camera (Dino-Lite Edge Am4815Zt, AnMo Electronics Corporation) to show the sample surface on a microscopic level.

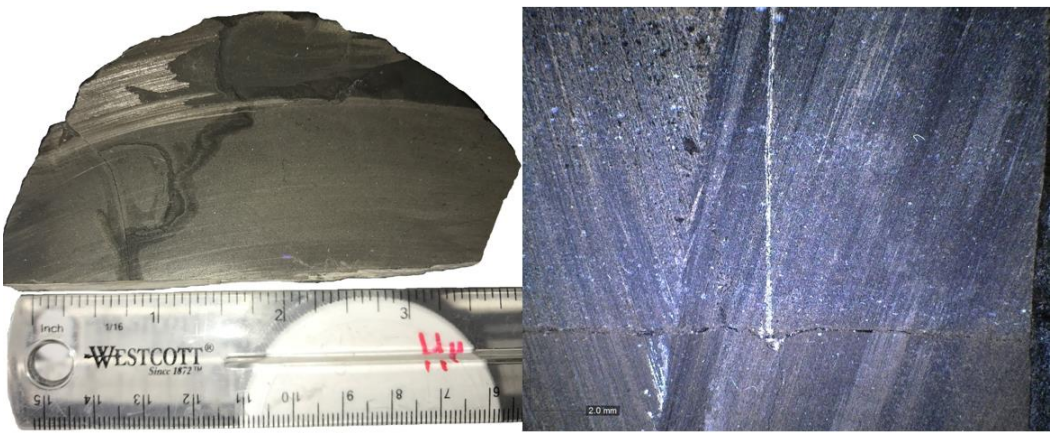




A8639

(2) (a)

(b)



A8722

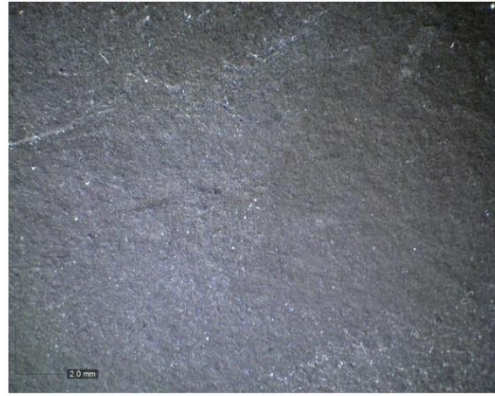
(3) (a)

(b)



A8829

(a)



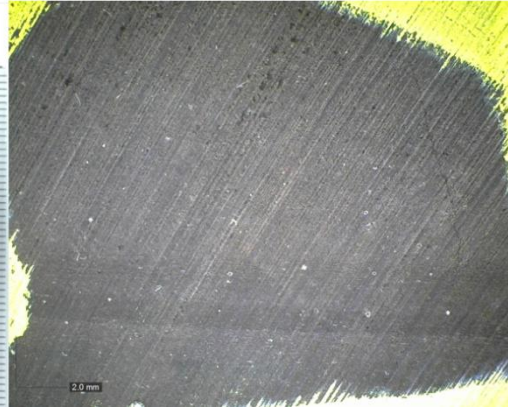
(b)

(4)



E6609

(a)



(b)

(5)



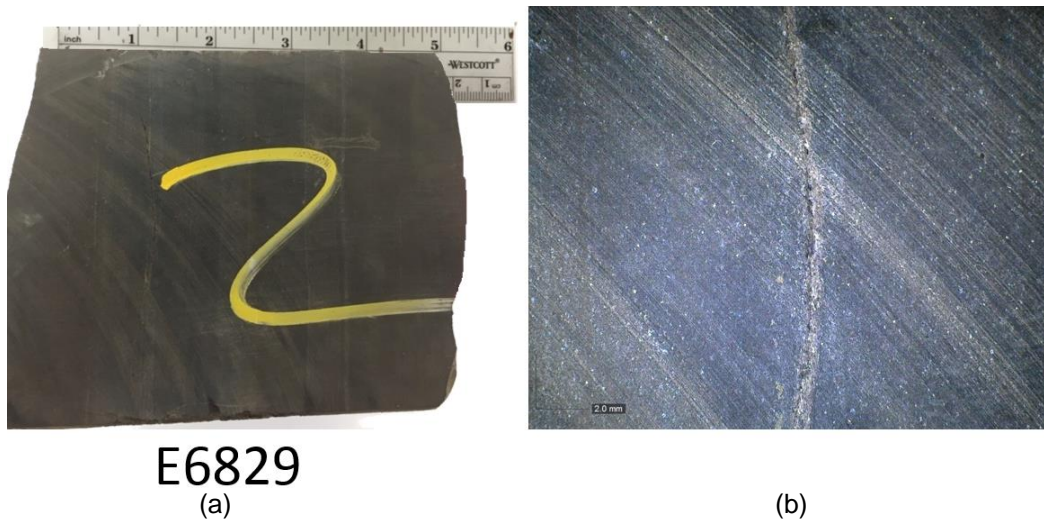
E6692

(a)



(b)

(6)



(7) Figure 3-1 Photos upon sample arrival: (a) Full sample taken with a digital camera (b) Sample surface taken at x20 zoom (scale bars are present in images at bottom-left corners, and the lamination looking marks in the photos are cutting marks)

The samples were then prepared for cutting by marking the lamination direction in red (used for orientation of samples during imbibition tests, not shown on pictures above). Two circular rock saws, one 12' blade and one 3' blade, were used to obtain 10 1cm x 1cm x 1 cm cubes at each sample depth, making 70 cubes in all. 18 of these cubes were used for fluid imbibition tests, 10 were used for MICP testing, and the remaining 42 were saved as backup. Imbibition tests need to be performed on a smooth and flat cube face which was indicated by a "B" for bottom. The letter "H", as well as a number 1-7, was then written on the opposite face indicating a horizontal/parallel orientation to lamination as well as the top of the sample (Figure 3-2). Neither H nor B is indicative of stratigraphic location. Quick-cure epoxy was then applied to each of the four remaining faces to facilitate fluid flow in one dimension. The changes in weight and dimensions were noted throughout this process. The ten cubes reserved for MICP testing were left un-epoxied. Before MICP and imbibition tests, the samples were placed in a 60°C drying oven for at

least 48 hours and then removed and cooled to room temperature (~22.5°C) in a desiccator.

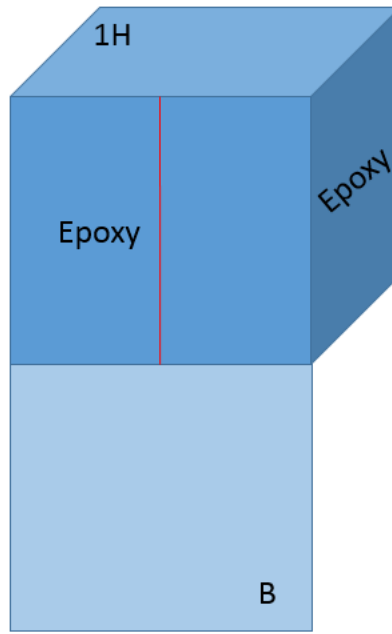


Figure 3-2 Example of epoxied cube indicating bottom face (to be in contact with imbibition fluid) and epoxied faces; number 1 indicates cube #1 while H indicates that imbibition direction will occur parallel (horizontal) to the bedding plane.

3-2 XRD and Geochemistry

Powder XRD (x-ray diffraction) analysis is performed to gather the mineral composition of the samples from different zones within the Woodford Shale. All samples were analyzed at the Shimadzu Center for Environmental Forensics and Material Science (called Shimadzu Center in this thesis) at the University of Texas at Arlington (UTA). At Shimadzu Center, samples crushed to a powder (<75 μm) were placed into a collimated monochromatic beam of x-radiation in the. The diffraction pattern is obtained and the quantitative mineralogy is determined by whole-pattern fitting using the Minerals

relational database, according to Shimadzu XRD-7000 Operating Instructions which can be found in Appendix A.

In order to measure the Total Organic Carbon (TOC), all samples were analyzed at Shimadzu Center and CUG (China University of Geosciences (Wuhan)). At the Shimadzu Center, Total Carbon (TC) and Inorganic Carbon (IC) are separately measured using a nondispersive infrared detector once acid was used to remove carbonates. IC values are then subtracted from TC values to obtain a TOC value. The standard operating procedures for TC/IC/TOC at Shimadzu Center can be found in Appendix B.

Pyrolysis analyses were performed on all samples at CUG. This analysis provides values for S1 (free hydrocarbons, mg HC/g; HC: hydrocarbon), S2 (hydrocarbons generated through thermal cracking, mg HC/g), S4 (amount of CO₂ produced during a combustion of pyrolysis residue, mg CO₂/g), T_{max} (the temperature at top of S2 peak, degree Celsius), and TOC (%). Note that TOC value is derived up to a temperature of 900 degrees Celsius, which probably does not account for whole carbon. From these values, parameters such as Production Index (PI), Bitumen Index (BI, normalized oil content), and Hydrogen Index (HI) can be calculated through the equations below (Johannes, 2006).

$$PI = S1 / (S1 + S2) \dots\dots\dots (3.1)$$

$$BI = (S1/TOC) * 100 \dots\dots\dots (3.2)$$

$$HI = (S2/TOC) * 100 \dots\dots\dots (3.3)$$

Vitrinite reflectance can be calculated based on an equation derived by Jarvie et al. (2001). This equation is derived using data from Barnett Shale and is being applied here due to the fact that both rocks contain type II kerogens.

$$\text{Calculated Ro \%} = 0.018 * T_{\text{max}} - 7.16 \dots\dots\dots (3.4)$$

3-3 Wettability and Contact Angle

Wettability tests are performed to investigate the wetting affinity of the Woodford Shale to de-ionized (DI) water (water-wetting), API (American Petroleum Institute) brine (water-wetting), 10 and 20% isopropyl alcohol (IPA, both water- and oil-wetting), and n-decane (oil-wetting). With a composition of 8% NaCl and 2% CaCl₂, API brine is used to mimic formation fluid and has a high salinity, while 10% IPA is used to achieve an intermediate surface tension between DI water and n-decane. Two types of wettability tests were performed, one with simply a hand held-pipette and microscopic camera (Dino-Lite Edge AM4815XT, AnMo Electronics Corporation) to video-record the spreading behavior, and the other with an optical dynamic/static interfacial tensiometer and contact angle meter (SI-200KB, KINO Industry). For both tests, slabs with dimensions 1cm x 1cm x 2mm were cut and then smoothed using 220 grit sand paper to remove cutting marks.

Two μL of fluid was dropped from a pipette onto a slab and then recorded from above for 30 seconds in order to observe the extent of liquid spreading. A qualitative number describing the extent of spreading was assigned to each liquid, with one representing no spreading at all and 10 representing complete spreading of the fluid across the slab. In regards to the contact angle at the droplet/sample surface interface, one represents a high contact angle values ($>100^\circ$) and 10 represents a low contact angle (~ 0). With Kino instrumentation 2 μL of fluid was dropped from a needle while a high speed camera recorded the process from a perpendicular view, allowing for the contact angle to be measured. This provided a quantitative analysis of the contact angle for each fluid.

3-4 Mercury Injection Capillary Pressure (MICP)

Mercury intrusion porosimetry is used to characterize the pore structure within each sample. This method uses non-wetting mercury to invade pore throats as small as three nanometers (Gao and Hu, 2013). In order to overcome the capillary pressure of increasingly small pores, a range of external pressure is applied up to 61,000 psia (420 MPa), using a Micrometrics Autopore IV 9510. During MICP testing, the sample undergoes both low- and high-pressure analyses. An equilibration time, or the minimum time duration to achieve a stable mercury intrusion level before moving to the next pressure value, was chosen to be 30 seconds for high-pressure analysis. In the end, a curve of pore-throat size distribution (PSD) is created with a range of 3 nm (dictated by the highest available pressure of the instrument) to about 50 μm (related to 5 psi filling pressure for a penetrometer suitable for sample porosity in the range of 5% commonly observed for shale). In addition to PSD, MICP characterizes a samples bulk density, particle density, porosity, total surface area, total volume, median pore-throat diameter, as well as permeability and tortuosity (Webb, 2001; Gao and Hu, 2013; Hu et al., 2015).

Mercury is a unique liquid in that it has a high surface energy and is nonwetting with respect to most geological materials. Assuming a cylindrical pore shape, the Washburn equation (Equation 3.5) can be utilized to convert the intrusion pressure to an equivalent pore-throat diameter (Washburn, 1921).

$$\Delta P = -\left(\frac{2\gamma\cos\theta}{r}\right) \dots\dots\dots (3.5)$$

Where,

ΔP – Difference in pressure across the curved mercury interface in a pore (psia);

γ - Surface tension for mercury (dynes/cm);

θ - Contact angle between the porous medium and mercury (degrees);

r – Pore-throat radius (μm).

The pore shapes are all assumed to be cylindrical which in nature is unrealistic for geological samples, but it provides a representation of pore distribution useful in petro-physical analyses. In the past both surface tension and contact angle have been assumed to be constant, even though surface tension of a liquid droplet is dependent on curvature and the contact angle varies with pore size. This stems from research on amorphous glass at the micrometer scale by Kloubek (1981), whose findings indicated that the error given by constant values was negligible, and the same was assumed for shale rocks. What was not taken into consideration was the importance of solid-liquid interactions at the nanometer scale. Once it was realized that shale characteristics exist heavily at this nm scale, Wang et al. (2016) developed a corrected Washburn equation (Equation 3.6) that incorporates variable contact angle and surface tension values as a function of pore size.

$$\Delta P = -\left(\frac{2\gamma_{Hg}(r) \cdot \cos\theta_{Hg}(r)}{r}\right) \dots\dots\dots (3.6)$$

Wang et al. (2016) reported that the error produced by the original Washburn equation grows in magnitude as pore sizes become smaller and smaller, making the modified equation essential in any shale analysis going forward.

The MICP approach can also be used to indirectly derive the permeability of the sample. Permeability is calculated using the Katz and Thompson equation given as Equation 3.7 (Katz and Thompson, 1986; 1987).

$$k = \left(\frac{1}{89}\right) (L_{max})^2 \left(\frac{L_{max}}{L_c}\right) \phi S(L_{max}) \dots\dots\dots (3.7)$$

Where,

k – Sample permeability to air (μm²);

L_{max} – Pore- throat diameter when hydraulic conductance is at a maximum (μm),
when mercury starts to percolate through the whole sample;

L_c – Pore-throat diameter (μm) corresponding to threshold pressure (psia) (taken from the inflection point on an intrusion curve);

ϕ - Porosity of the sample (%);

$S(L_{\text{max}})$ – Mercury saturation at percolation for L_{max} (Gao and Hu, 2013).

Lastly, tortuosity quantifies the ability of fluid to move through tortuous pore networks and it can be calculated by inputting MICP data into Equation 3.8 (Hager, 1998; Webb, 2001; Hu et al., 2015).

$$\tau = \sqrt{\frac{p}{24\kappa(1+pV_{\text{tot}}) \int_{\eta=r_{c,\text{min}}}^{\eta=r_{c,\text{max}}} n^2 f_v(n) dn}} \dots\dots\dots (3.8)$$

Where,

τ - Tortuosity (dimensionless);

p – Grain density of sample ($\frac{g}{\text{cm}^3}$);

V_{tot} – Total pore volume ($\frac{\text{ml}}{g}$);

r_c – Capillary radius (μm);

$f_v(r_c)dr_c$ — volume probability density function (volume of pores with a radius in the range of r_c to $r_c + dr_c$ per kg of dry material) , cm^3/g ;

$r_{c,\text{min}}$: minimum detectable capillary radius by MICP, μm ;

$r_{c,\text{max}}$ —maximum detectable capillary radius by MICP, μm ;

$\int_{\eta=r_{c,\text{min}}}^{\eta=r_{c,\text{max}}} n^2 f_v(n) dn$ – Pore-throat volume distribution by pore-throat size.

Procedure for MICP Tests

The shale samples are oven dried at 60°C for 48 hours to remove moisture. Then they are removed and immediately placed inside a desiccator with less than 10% humidity to be cooled to room temperature (~22.5°C). Once cooled, the sample is placed into a penetrometer, which is an apparatus with a sample chamber connected to a metal

precision-bore and glass capillary system. The penetrometer is properly sealed with vacuum grease and placed into the low-pressure chamber where it is evacuated to 6.7 Pa (0.05 torr, 0.000972 psi, 50 μm Hg, or 99.993% vacuum) in order to clear the samples' pore network of air and moisture. Once a near vacuum is achieved the sample undergoes low-pressure intrusion analysis, which involves filling the penetrometer with mercury to a pressure of 5 psia (0.034 MPa) to envelop the cubic sample and calculate bulk and grain densities by keeping track of mercury volume/weights. Then as the mercury invades the sample with increasing pressures, it overcomes the capillary pressure of pore throats averaging 50 μm , which can change based on the type of penetrometer to accommodate different (e.g., more porous) samples. Equilibrium time is then given in order for the intruded mercury volume to stabilize ($<0.1 \mu\text{L}$) at a specific pressure level before the next pressure is applied; the equilibrium time during low-pressure analysis is set to 10 seconds.

Once low-pressure analysis is complete, the penetrometer is placed in the high-pressure analysis chamber. During high-pressure analysis, the pressure incrementally increases from 30 psia to 61,000 psia with an equilibrium time of 30 seconds for each pressure increment where the mercury volume is monitored at a detection limit of $< 0.1 \mu\text{L}$. At its highest pressure, mercury can invade pore throats as small as 2.8 nm, according to variable contact angle and surface tension method of Wang et al. (2016). One cautionary note is that "while MICP is widely accepted as the standard approach in determining pore-size distribution, the ink-bottle phenomenon [large-sized pores are connected by smaller pore throats] and pore accessibility issues [only pores connected to the sample edge are accessible for mercury intrusion] cause it to underestimate the volume of large pore and overestimate that of small pores" (Hu and Ewing, 2014). The ink-bottle shaped pores describe the model used by MICP analysis of large pores

connected by smaller neck entrances from the sample surface. In the meantime, MICP analyses provide information about connected pore network that is complementary to other methods. The MICP data are presented in a report format by the Autopore program which is then processed using Microsoft excel to provide the charts and figures presented in this thesis.

3-5 Fluid Imbibition

According to Gao and Hu (2012), “spontaneous imbibition is the process during which the nonwetting fluid (air) in a porous medium is displaced by a wetting fluid (water or n-decane) due to capillary pressures”. Imbibition data can be correlated with variations in permeability, porosity, boundary conditions and liquid viscosity ratios (Morrow et al, 2001), and illustrate the pore connectivity of a rock (Hu et al., 2012). Samples were epoxied and dried in preparation for the tests. A fluid uptake experiment (imbibition) was done using two different fluids, DI water and n-decane. The samples were suspended from a bottom-weighing electronic balance (Shimadzu Model AUW220D, at a precision of 0.00001 g) located inside a chamber with a reservoir (glass Petri dish) resting on its floor. The humidity in the chamber was measured at roughly 98% due to the hole in the chamber to let the suspension wire from the balance run through. The chamber could be raised and lowered on a support jack, and to begin the experiment by lowering it so that 1 mm of the sample was in contact with fluid (Figure 3-3).

Balance readings were then recorded as frequently as one second. Before each run, the sample was weighed along with the reservoir plus solution, sample holder, and sample plus holder. At the end of each run the sample was lifted out of the reservoir and excess fluid was wiped from the sample with a tared moist Kimwipe of a specific fluid being tested. The sample and Kimwipe were then weighed separately as well as the weight changes of the sample and the reservoir for mass-balance analyses. Fluid

unaccounted for was treated as evaporative loss and an estimated evaporative loss was achieved through blank experiment without a sample (Hu, et al., 2001).

DI water imbibition tests were run at durations of 6, 10, 12, and 24 hrs depending on the sample. A single n-decane imbibition test was run on each sample for 6 hrs. In total, 18 imbibition tests were run for this work.

Previous modeling work by Ewing and Horton (2001) based on the percolation theory indicates that rocks with a well-connected pore space will have a fluid front advancing with the square root of time, while rocks with a poorly connected pore space will have a fluid front that advances at one fourth the power of time. This relationship gives a slope of 0.5 and 0.25 respectively in log space which is called the imbibition slope in this thesis. Higher slopes are generally recorded at the beginning of the tests as edge-accessible porosity is a factor when the sample first comes in contact with the fluid. As time goes on, the fluid is solely interacting with the interior pore space and the slope decreases. The slope achieved by these tests gives valuable insight into the samples pore space connectivity.

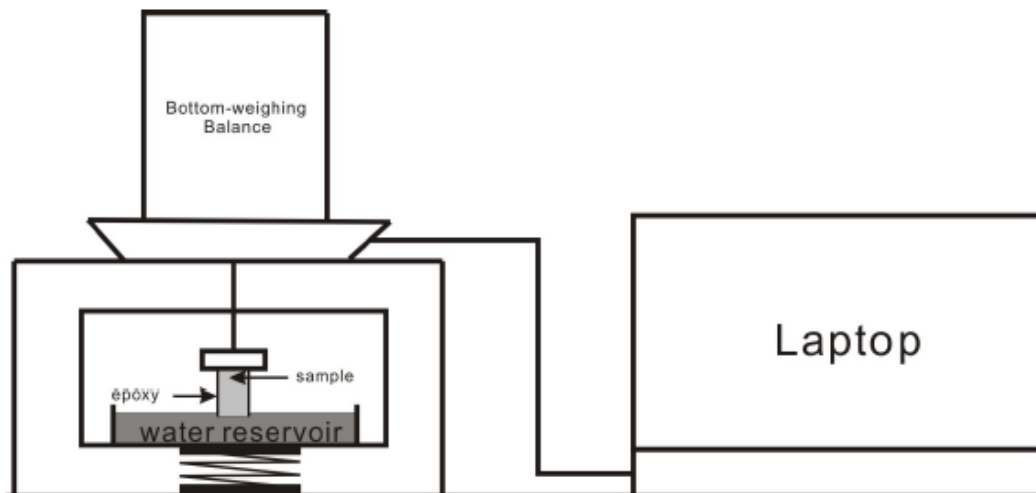


Figure 3-3 Schematic of the Apparatus for Imbibition Test (Gao & Hu, 2012)

3-6 Log Analysis

Well logs provide direct measurements of the rock properties encountered in a borehole making them necessary for regional correlation and mapping. The raw data can be further processed to provide several rock characteristics looked at in this study. Both the digital and raster logs used for this study were provided by the company. Further interpretation and calculations were performed using UTA facilities and Petra licenses provided by UTA from IHS. Both wells A and E are horizontal wells and so the section of the Woodford analyzed exists within the curve of the well and therefore the thickness is exaggerated to a small extent.

Porosity results can be obtained from density logs which can be used to calculate the bulk density of the rock they encounter. The most common combination of logs to look at when trying to estimate the porosity of a reservoir is a neutron-density crossplot porosity log. The problem with these logs is that they tend to over- or under-estimate the total porosity of the rock (Smithson, 2012). When a density log encounters rock with a large amount of organic materials such as shale, it will overestimate the porosity since it is commonly calibrated on a limestone matrix, which has a higher density than organic matter. In order to compare log-calculated porosities with porosity measurements from core samples, a recalibration is needed. This can be achieved by looking at the TOC data collected from the core. For high TOC readings, the subsequent porosity reading should be adjusted using a lower matrix density. This is done through a process of trial and error using core and log data from Well E. Three matrix density values are analyzed to obtain a density-porosity curve that best mimics the porosity data from the core. Equation 3-10 below is used to convert density porosity to a corrected porosity (Anovitz and Cole, 2015).

$$\phi = \frac{\rho_m - [(1 - \phi_d) * \rho_{ls} + \phi_d]}{\rho_m - 1} \dots \dots \dots (3.10)$$

Where,

- ϕ – Porosity (%);
- ρ_m – Assumed matrix density (g/cm³);
- ϕ_d – Density porosity from log (%);
- ρ_{ls} – Limestone density (g/cm³);

Water saturation is important as it can provide insight into what type of fluid is occupying the pores. The higher the water saturation, the more likely the pores are filled with water and not hydrocarbons (Morris and Biggs, 1967). In order to create a curve for water saturation, different variables need to be obtained relating to the modified Archie's Equation (Masoudi et al., 2011), shown as Equation 3.11.

$$S_w = \left(\frac{R_w}{R_t * \phi^m} \right)^{\frac{1}{n}} \dots \dots \dots (3.11)$$

Where,

- S_w – Water saturation (fraction);
- R_w – Formation Water resistivity (ohm m);
- R_t – Deep resistivity measured from logs (ohm m);
- ϕ - Cross-plot porosity (%);
- m – Cementation factor (dimensionless);
- n – Saturation exponent (dimensionless).

For both wells, deep resistivity curves (measure resistivity past the zone intruded by drilling mud) were used for true resistivity while the density porosity curve was used for cross-plot porosity values. For simplicity, a value of 2 was used for both the cementation and saturation factor due to the high cementation and salinity of the formation brine which may cause an over- or under-estimation of water saturation (Bennion et al, 1996). There

were no formation water tests available in the basin, so two water resistivity values were used to create two curves. The first value was 0.04 ohm m, a common resistivity measurement for a brine at these depths. The second water resistivity value was based on the water saturation values measured from the core.

In addition to porosity, permeability is another important value to look at when evaluating the hydrocarbon production potential of a reservoir. In order to obtain permeability values based on the porosity values measured from the density porosity log, a relationship was developed between the porosity and permeability values measured through MICP in this work. The equation provided based on the trend line of this data is listed below as Equation 3.12.

$$\kappa = 0.000002 * \phi - 0.0000005 \dots\dots\dots (3.12)$$

κ = Permeability (mD)

ϕ = Corrected porosity from density porosity log (%)

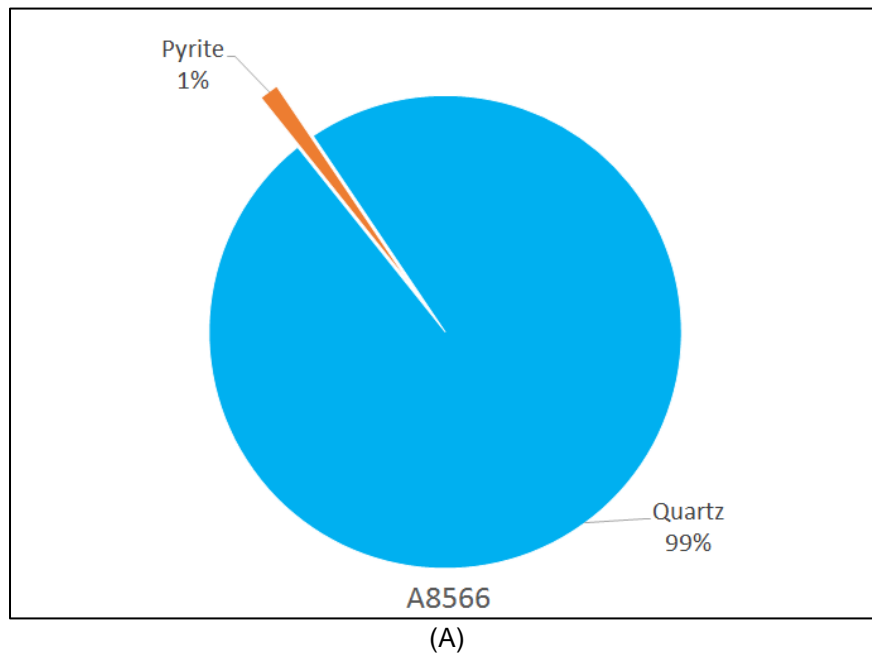
3-7 Production Data

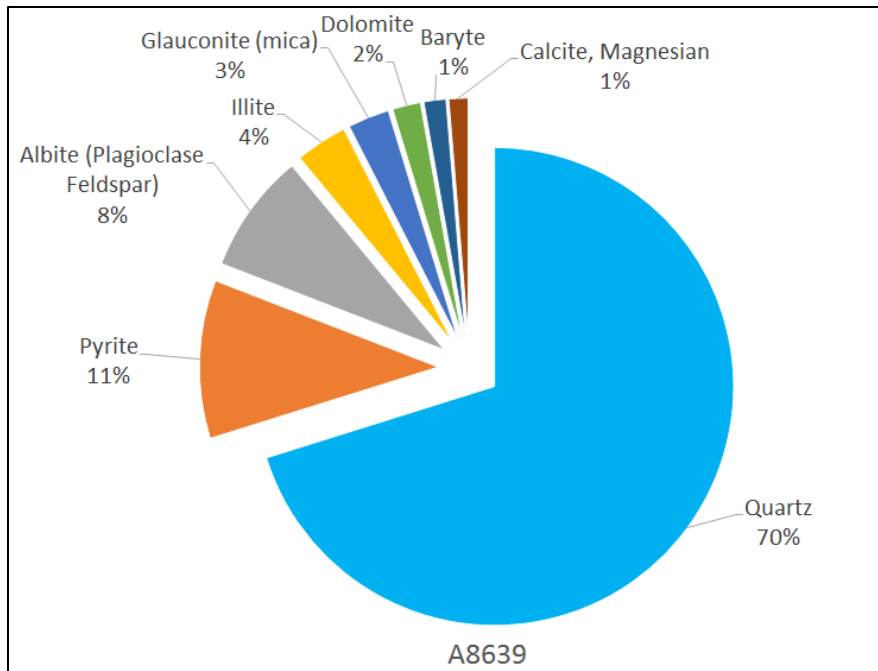
DrillingInfo gathers production data on a monthly basis from the Oklahoma Corporation Commission, the state regulatory agency for oil and gas industry in Oklahoma. Using a complimentary subscription of DrillingInfo Pro version provided to UTA, production data can be quickly viewed and utilized for this work.

Chapter 4 Results

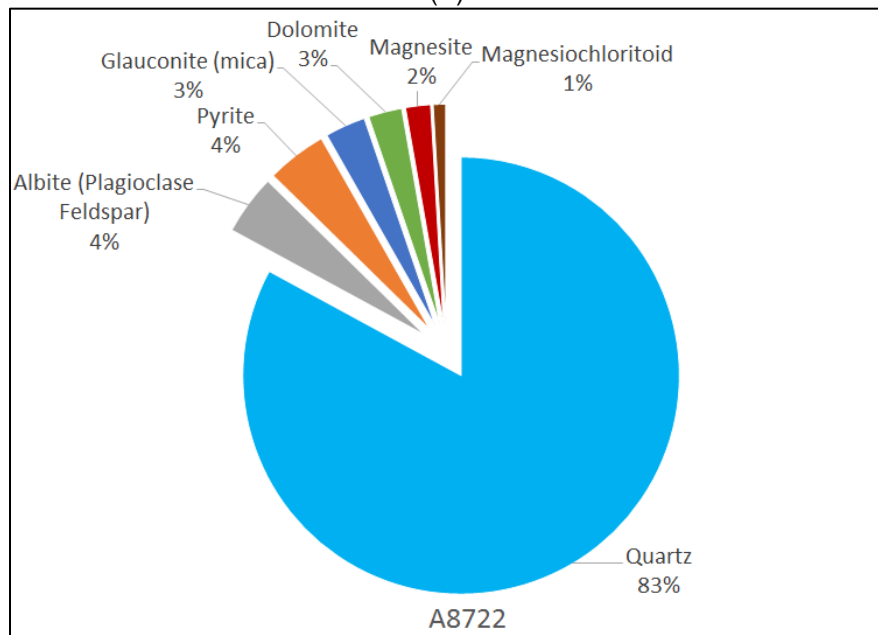
4-1 Mineralogy and Geochemistry

The mineral composition of the samples is mostly quartz rich (Figure 4-1 and Table 4-1). Within a range from 6 to 18%, clay minerals are the second most common constituent, present in 4 of the 7 samples. After plotting the samples on a lithology diagram (Figure 4-2), 6 of the 7 samples have a silica-dominated lithotype while one sample (A8829) is a clay-rich siliceous mudstone.

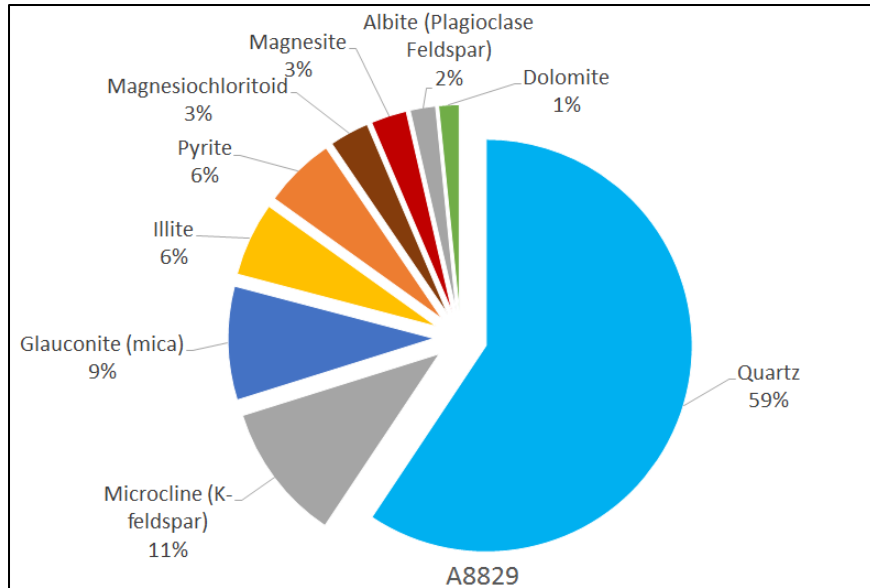




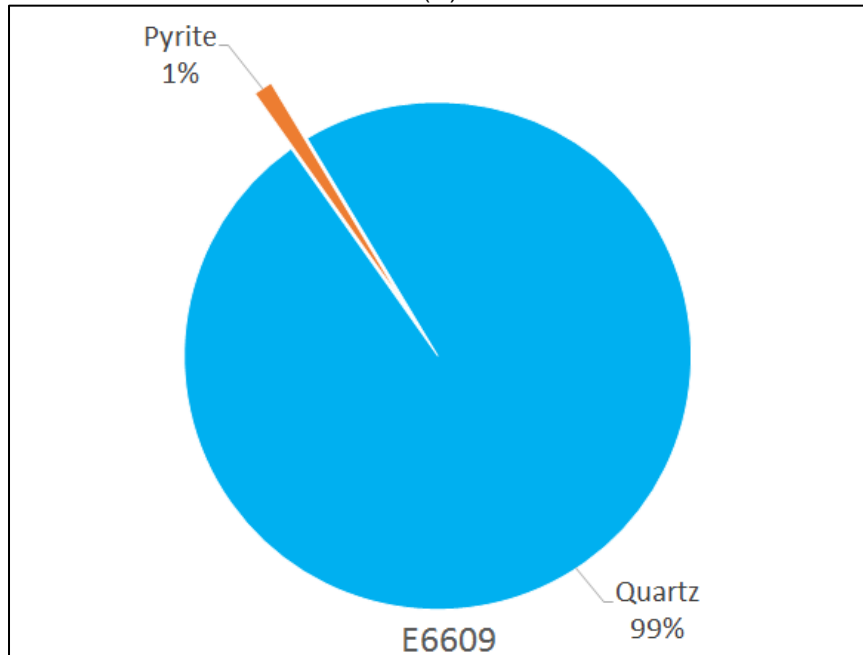
(B)



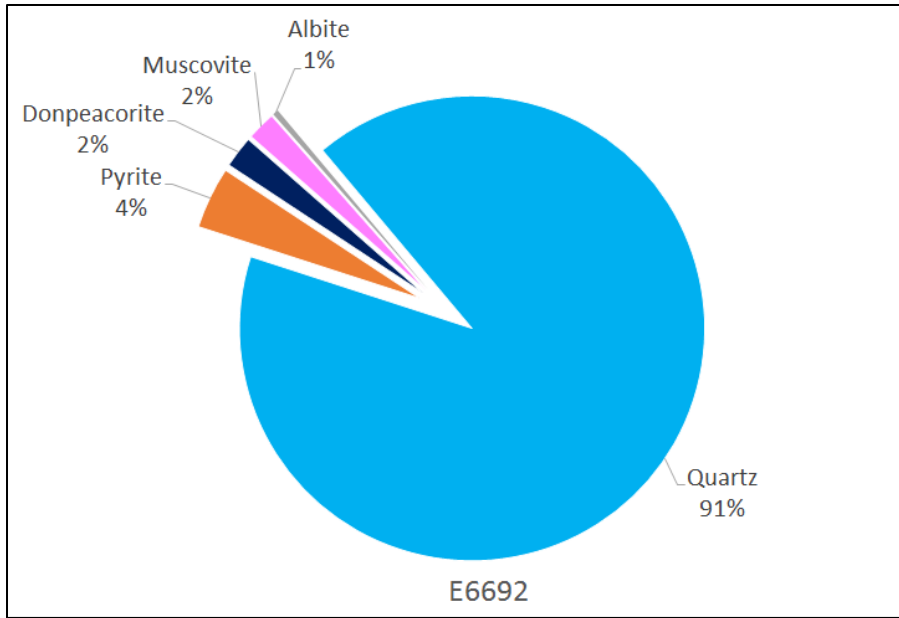
(C)



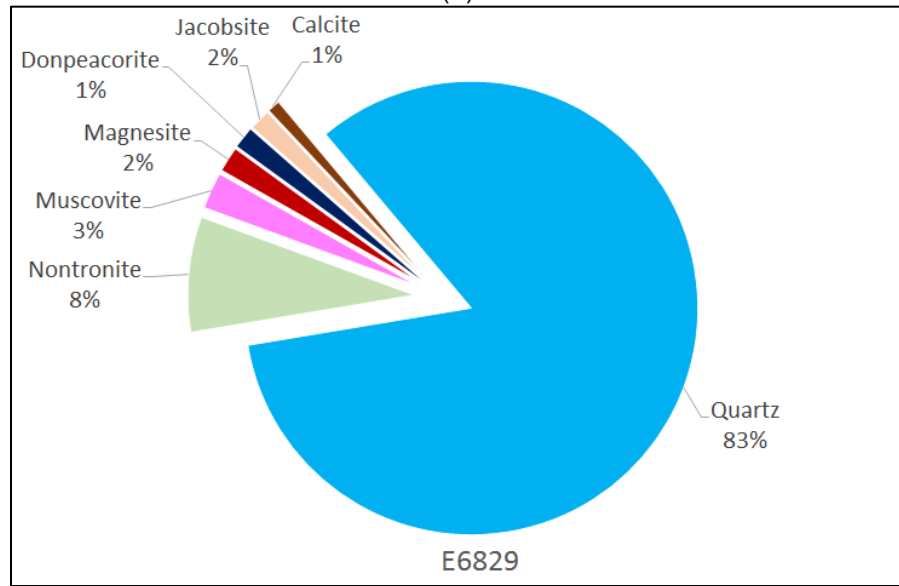
(D)



(E)



(F)



(G)

Figure 4-1 X-ray Diffraction (XRD) Results for Samples from Well A (A-D) and Well E

(E-G)

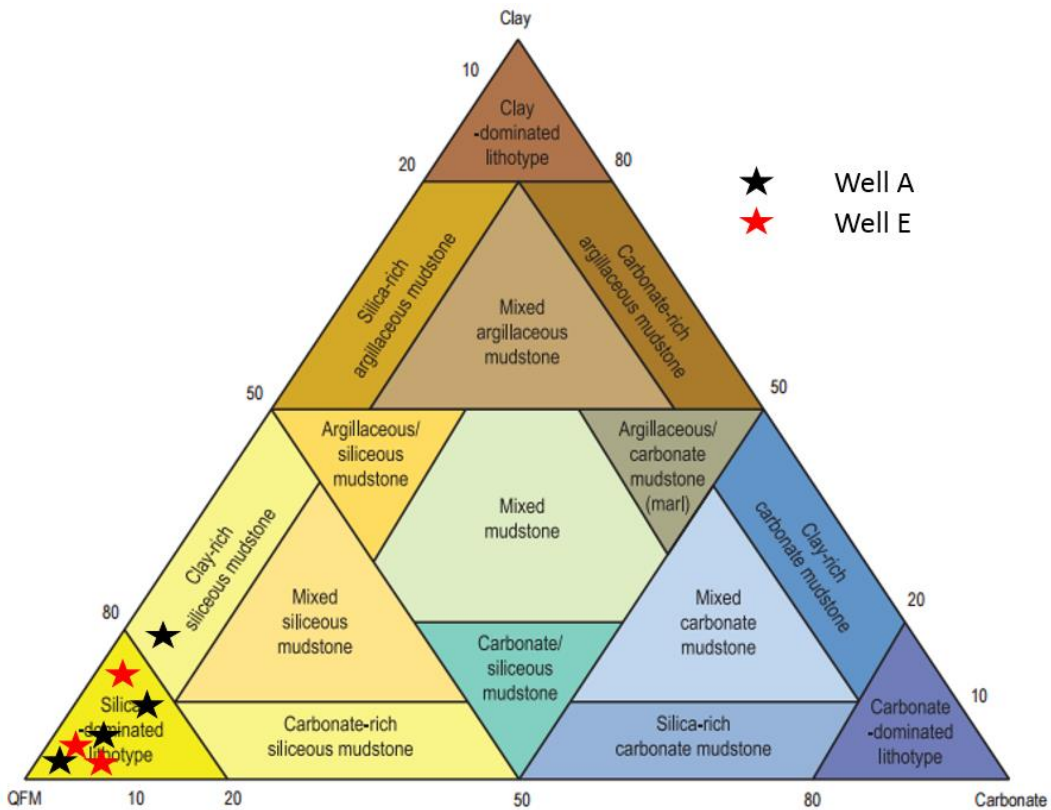


Figure 4-2 Diagram for sCore Lithofacies Classification Scheme for Organic Mudstones for Wells A and E

Table 4-1 Summary of XRD results obtained from Shimadzu Center

Phase	A8566 (%)	A6839 (%)	A8722 (%)	A8829 (%)	E6609 (%)	E6692 (%)	E6829 (%)
Lithofacies	Silica Dominated	Silica Dominated	Silica Dominated	Clay-Rich Siliceous Mudstone	Silica Dominated	Silica Dominated	Silica Dominated
Quartz	99	70	81	59	99	91	83
Albite	-	8	4	2	-	-	-
Microcline	-	-	-	11	-	-	-
Donpeacorit	-	-	-	-	-	2	2
Pyrite	1	11	4	6	1	4	-
Baryte	-	2	-	-	-	-	-
Jacobsite	-	-	-	-	-	-	2
Calcite	-	1	-	-	-	-	1
Dolomite	-	2	2	2	-	-	-

Magnesite	-		2	3	-	-	2
Illite	-	4	3	6	-	-	-
Glauconite (mica)	-	3	3	9	-	-	-
Nontronite (smectite)	-	-	-	-	-	-	8
Magnesioclhoritoid	-	-	1	3	-	-	-

The pyrolysis data acquired for this study is presented in [Table 4-2](#). Pyrolysis data are used to assess the quality and quantity of present-day organic matter for the Woodford Shale. S1 values range from 2.43 to 5.96 mg HC/g, with a general trend of increase with depth. S2 values range from 14.2 to 46.3 and do not follow a particular trend. T_{max} values range from 428 to 437, indicating that the organic matter exists at immature to early maturity levels ([Carvajal-Ortiz and Gentzis, 2015](#)). This indicates largely oil production, but the wells are still producing gas. The gas has most likely migrated up through the large thrust fault that separates the shallow and deep Ardmore basin. TOC values from the pyrolysis tests range from 3.82 to 10.1% with no trends. Kerogen type is displayed in [Figure 4-3](#) and was chosen based on the hydrocarbon index values and portrays the samples as mostly Type II ([King, 2015](#)). The relationship between S1 and TOC values can be an indication of the hydrocarbon content of the shale ([Jarvie, 2012](#)). When both values are plotted with depth, a crossover of the oil content relative to organic richness identifies sections of reservoir that contain potentially producible hydrocarbons. This crossover also indicates the point at which the bitumen index reaches 100 mg hydrocarbons TOC ([Jarvie, 2012](#)). [Figures 4-4 and 4-5](#) below illustrate these effects.

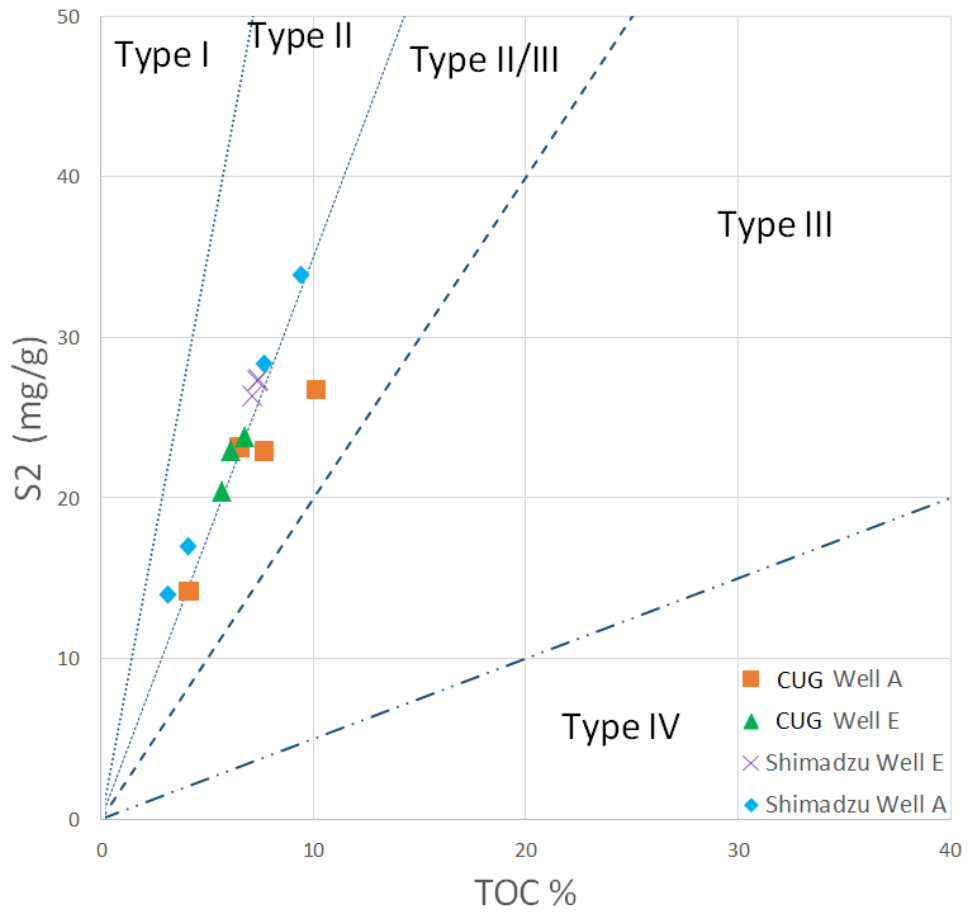


Figure 4-3 S2 vs. TOC, Partitioned by Kerogen Type, and Colored by Laboratory where Results were Collected

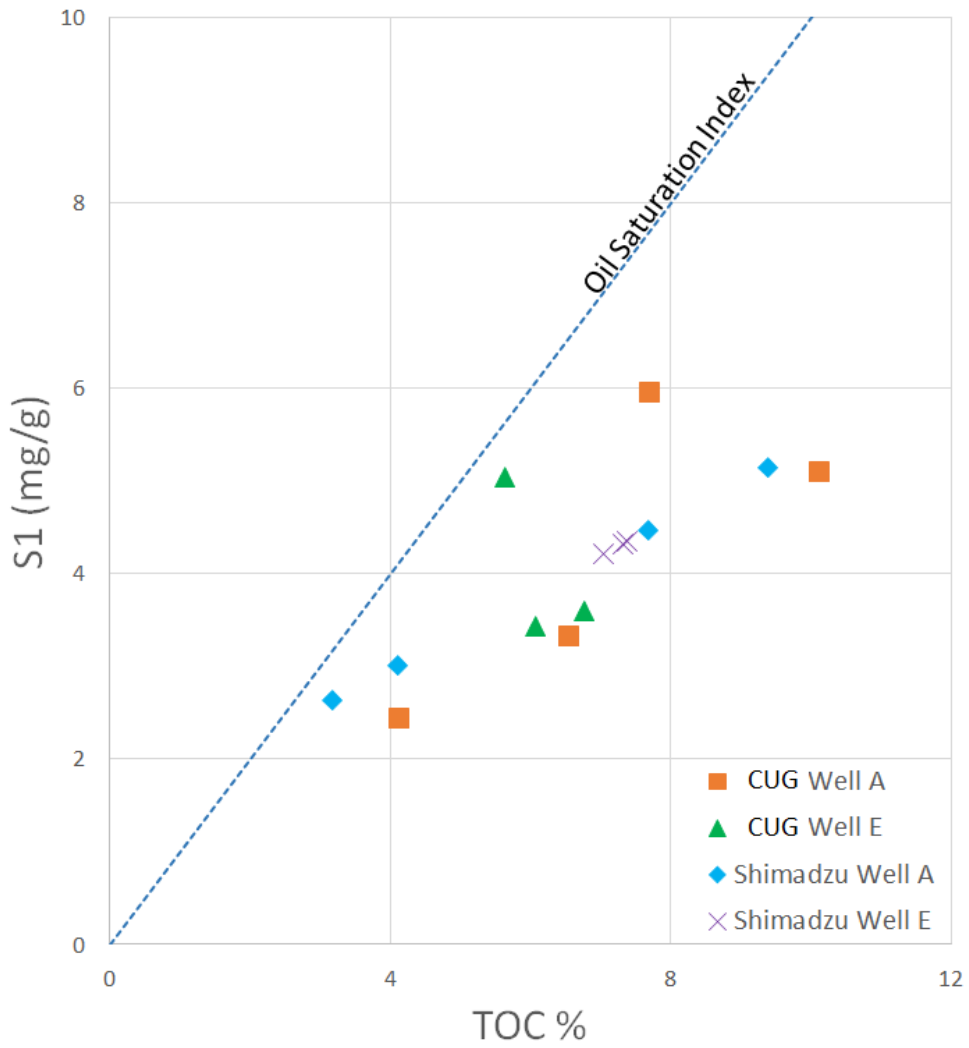


Figure 4-4 S1 vs TOC with Oil Crossover, Colored by Laboratory Analysis

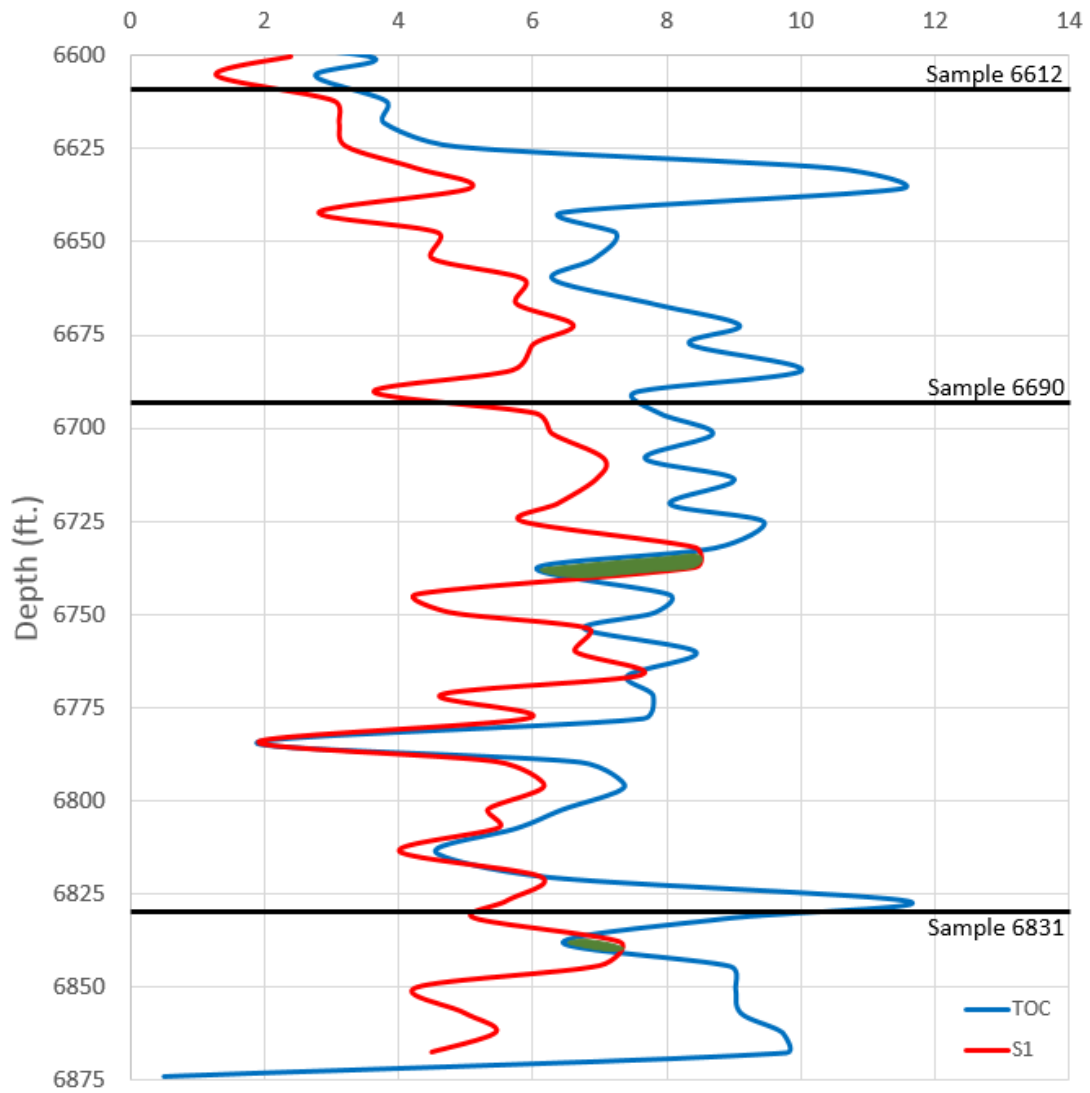


Figure 4-5 Depth vs. TOC (wt%) and S1 (mg HC/g rock), Oil Crossover Shaded in Green, for Well E RTC data

Table 4-2 Pyrolysis Results

	China University of Geosciences (Wuhan)						
	A8566	A8639	A8722	A8829	E6609	E6692	E6829
S1 (mg HC/g)	3.33	5.11	5.96	2.43	3.60	3.44	5.05
S2 (mg HC/g)	23.2	26.8	22.9	14.2	23.8	22.9	20.5
S4 (mg CO₂/g)	43.3	74.8	53.0	27.6	44.8	38.9	35.2
TOC (%)	6.53	10.13	7.70	4.14	6.75	6.08	5.64
T_{max} (°C)	435	433	433	428	435	433	433
HI (mg HC/g TOC)	355	264	298	343	353	377	363
PI	0.126	0.16	0.206	0.146	0.131	0.131	0.198
BI (%)	51	50	77	59	53	57	90
Kerogen Type	Type II	Mixed II/III	Mixed II/III	Mixed II/III	Type II	Type II	Type II
Calulated Ro (%)	0.670	0.634	0.634	0.706	0.67	0.634	0.634
TOC Measured at Shimadzu (%)	4.11	9.39	7.68	3.17	7.37	7.04	7.54

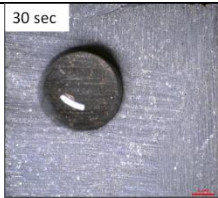
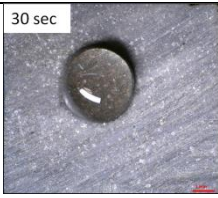

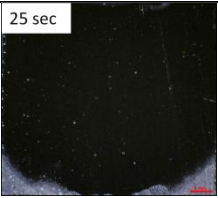
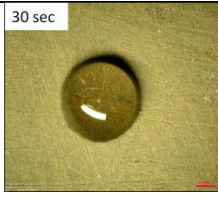
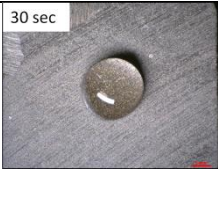



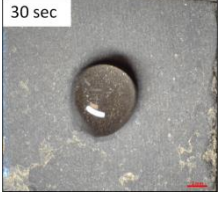
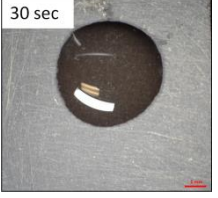
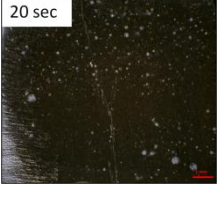
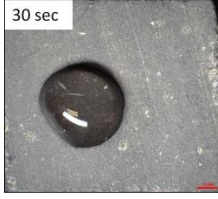
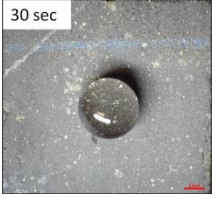
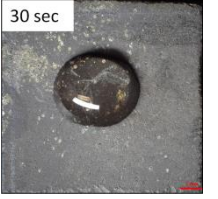
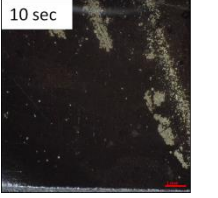
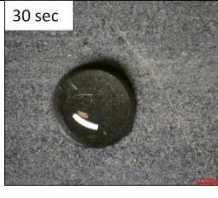


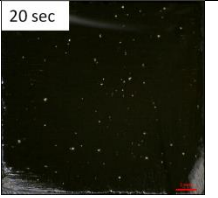
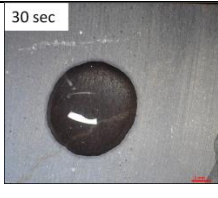

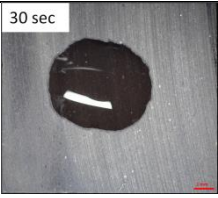
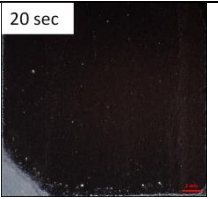
4-2 Wettability

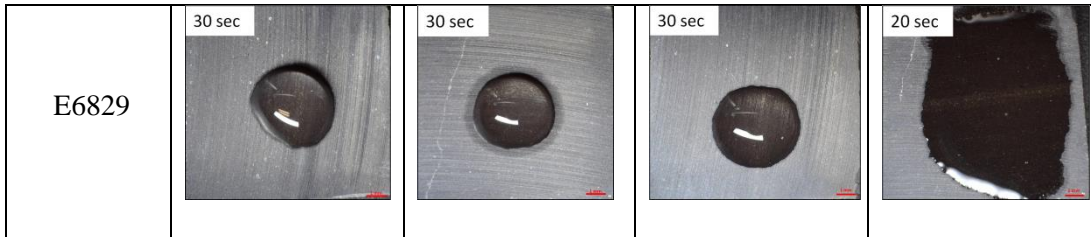
The qualitative wettability index results are presented in Table 4-3 with the corresponding images in Table 4-4. Observing either the hydrophilic or hydrophobic characteristics of each fluid helps determine the wetting behavior of each shale sample. When a droplet of DI water was applied to each sample, a wettability index range from one to three was obtained. These low values indicate non-water wetting characteristics for all seven samples. To further support this, the wettability index range for n-decane was from eight to ten, where a complete spreading is defined at ten. This phenomenon is most likely due to the affinity of n-Decane to the organic matter (e.g., kerogen) phase which is microns in size and dispersed throughout the samples. In order to observe a complete range of wetting fluids, both API brine and a 10% IPA were applied to the samples as well. The wettability index range for both fluids remained low, providing a skewed view of wettability for these samples.

Table 4-3 Qualitative Droplet Wettability Result

Sample ID	Wettability Drop Test (2 μ L)			
	DI	API Brine	10% IPA	n-Decane
A8566	1	2	3	10
A8639	2	1	3	10
A8722	1	1	3	10
A8829	2	1	2	10
E6609	2	1	3	10
E6692	3	4	5	10
E6829	2	3	4	8

Table 4-4 Droplet Wettability Images

Sample ID	DI Water	API Brine	10% IPA	n-Decane
A8566				
A8639				
A8722				
A8829				
E6609				
E6692				



In order to obtain a full view of the wetting characteristics, a 20% IPA, instead of a 10% IPA, was used in the quantitative analysis done with the contact angle analyzer. The results for each sample are provided in graphical form below in [Figure 4-6 a-g](#) and in [Tables 4-5 and 4-6](#). Most samples produced the same results as the qualitative test performed using a microscopic camera at UTA. The contact angle for DI water fluid/sample pair was the highest (from 58.5 to 109) indicative of hydrophobic behavior, while the n-decane/sample contact angle was low (0) indicating hydrophilic behavior and complete spreading at the mm-range observable scale. For samples A8722 and A8829, the contact angle of the API brine was actually higher than that of the DI water. [Gomari and Joseph \(2016\)](#) found that clay content plays a significant role in producing higher contact angles for brines, and this could explain the higher contact angles produced by brines in samples A8722 and A8829.

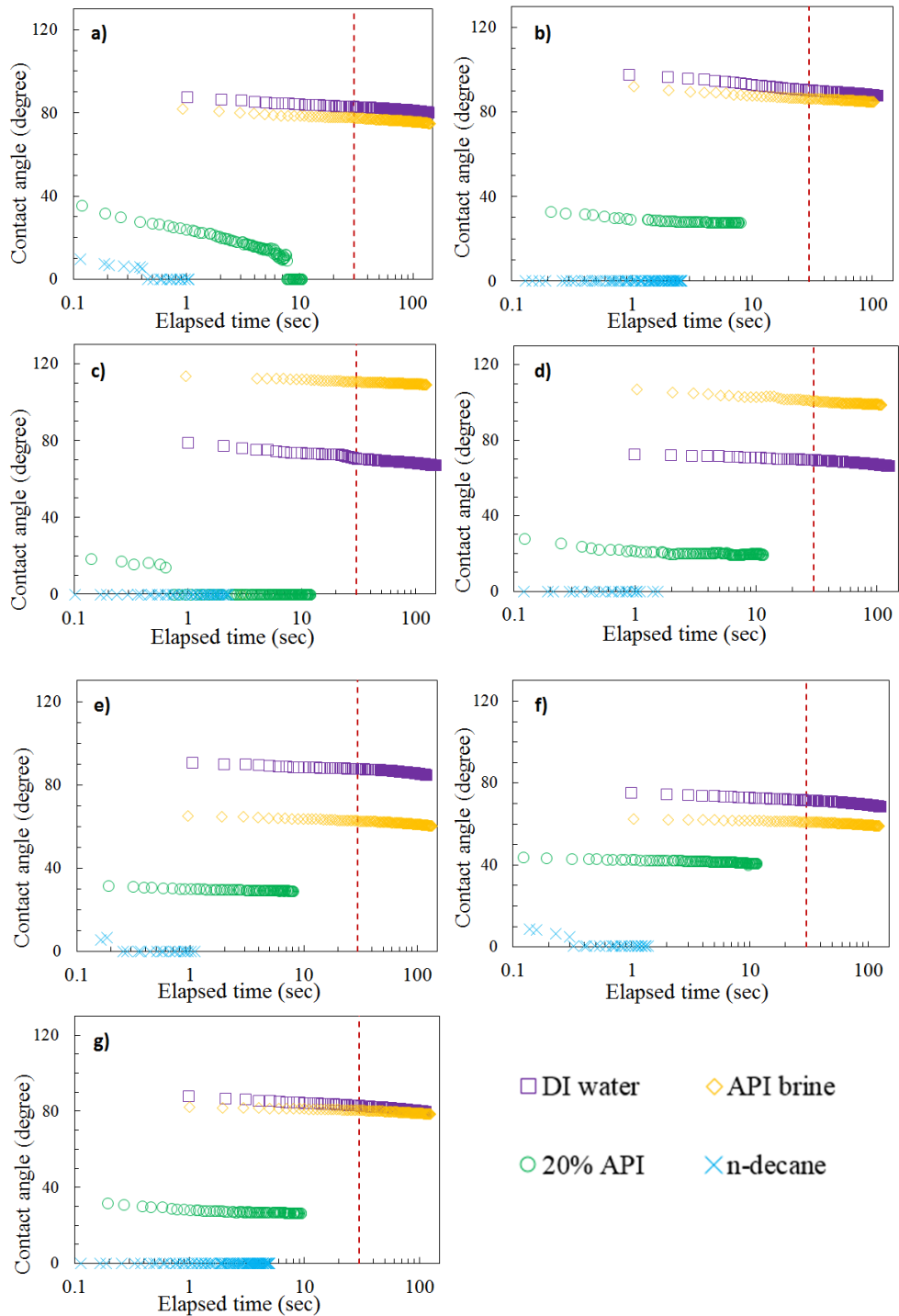
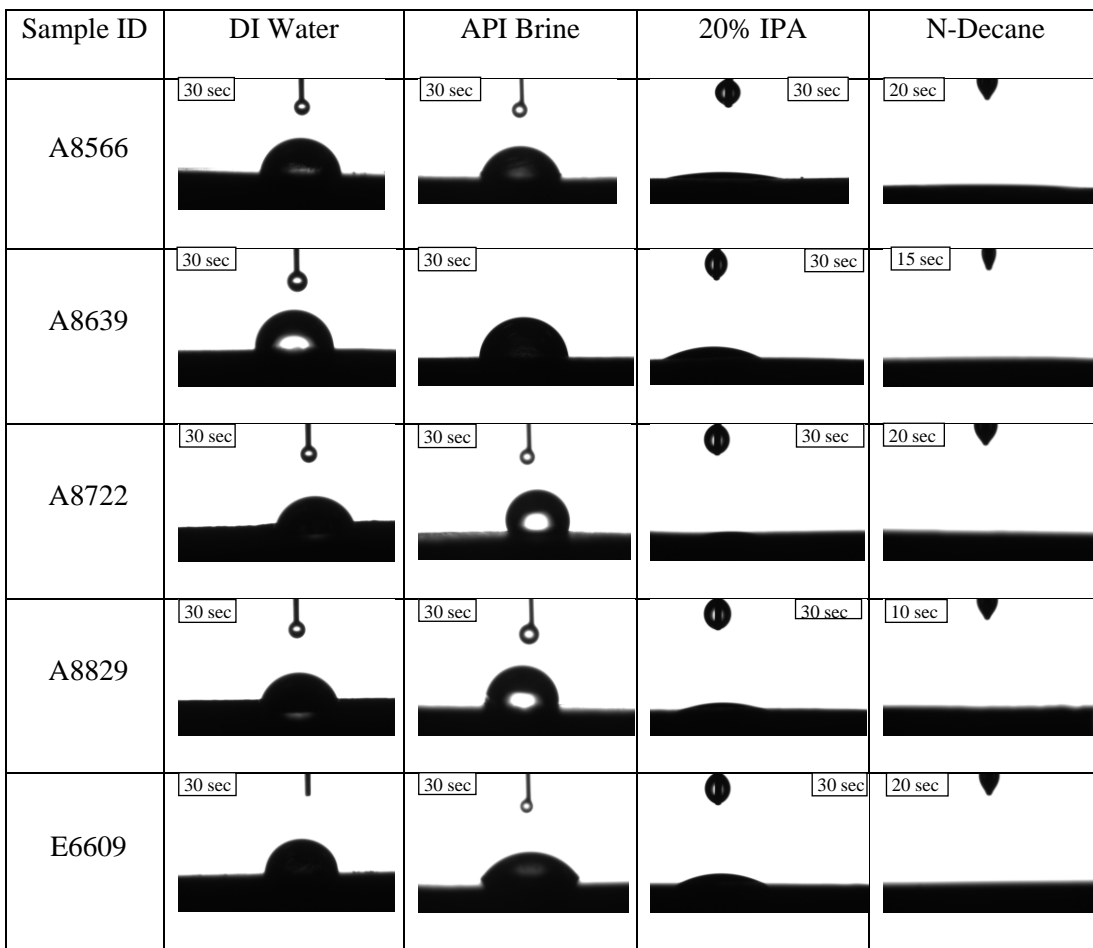


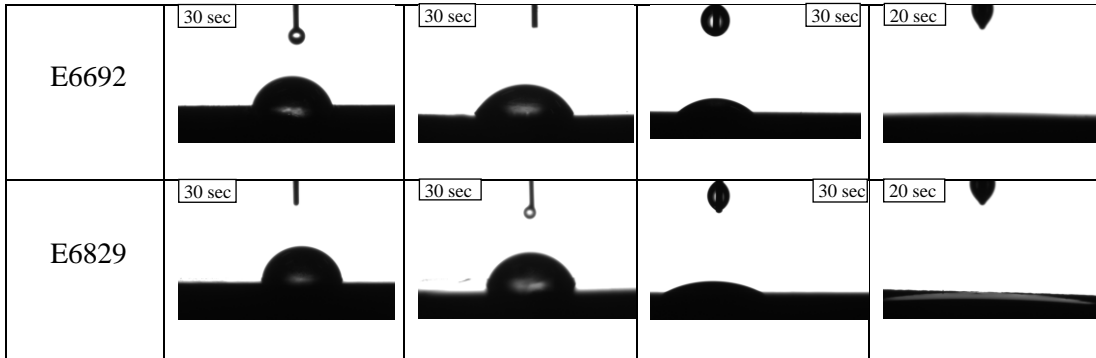
Figure 4-6 Contact Angle Measurements a) A8566 b) A8639 c) A8722 d) A8829 e) E6609 f) E6692 g) E6829

Table 4-5 Compilation of Contact Angles

Sample ID	Contact angle (deg)			
	120 sec DI	120 sec API brine	120 sec 20% IPA	10 sec n-Decane
A8566	81.3	75.7	0	0
A8639	87.7	84.7	27.5	0
A8722	65.4	109	0	0
A8829	66.4	98.9	19	0
E6609	84.8	60.3	28.9	0
E6692	68.5	58.5	40.6	0
E6829	79.7	78.5	26.3	0

Table 4-6 Wettability 2 μ L Images





4-3 Mercury Injection Capillary Pressure (MICP)

MICP testing was performed according to the methods outlined in Chapter 3. The test measures the volume decrease at which mercury invades the samples under each pressure step in order to provide a pore-throat size distribution profile. Other petrophysical properties such as bulk density, porosity, permeability, and tortuosity can also be calculated using the results of this test.

Total pore area of all samples covers a range of 1.2 – 4.6 m²/g without a general trend with depth or formation location. Porosity values range from 0.85 to 3.09 % with Well A samples producing the higher porosity values between the two wells. Bulk density values range from 2.31 g/cm³ (sample A8829) to 2.45 g/cm³ (samples A8566 and E6609).

Inflection points within the MICP data represent the moment at which the capillary pressure starts to percolate across the whole sample through a connected pore network controlled by a pore-throat size. Each inflection point is chosen to represent a connected pore network, and the sample-specific percentages of these pore sizes are shown in [Table 4-7](#). The pressure values recorded during MICP runs are used in the modified Washburn equation of Wang et al. (2016) to calculate the pore-throat size distribution for each pressure. An example of selected reflection points for a sample (A8829) can be seen [in Figure 4-7](#). From pressure-volume data, both permeability and

tortuosity values can be calculated. In order to capture the most representative permeability and tortuosity values for each sample, the pore size range with the greatest percentage of pores was chosen and the values are outlined in **Table 4-8**. Permeability values range from 4.415×10^{-7} mD to 1.529×10^{-5} mD while tortuosity values (a dimensionless measurement of the degree of non-linearity of the pathways in the sample) range from 829 to 19829.

Table 4-7 Pore-throat Size Distribution (%); A, B, C denotes replicate analyses

Sample ID	Pore-throat Size (μm)						
	0.0028-0.005	0.005-0.01	0.01-0.05	0.05-0.1	0.1-1	1-10	10-50
A8566 A	26.0	27.5	19.3	3.60	5.30	8.30	9.90
A8566 B	23.5	26.7	19.3	3.30	5.00	8.90	13.2
A8639	26.9	29.4	22.2	4.70	5.90	3.70	1.60
A8722	0.00	34.1	38.5	7.40	10.8	6.10	3.10
A8829	22.2	28.0	26.1	4.30	5.50	6.60	7.30
E6609	28.5	25.3	22.2	4.80	4.10	10.3	4.90
E6692	24.0	25.8	22.9	4.23	6.70	10.1	6.30
E6829 A	24.8	31.2	25.4	4.78	4.60	3.90	5.20
E6829 B	3.90	34.7	30.6	5.07	5.30	11.0	9.30
E6829 C	19.1	19.0	36.4	6.33	6.70	5.70	6.80

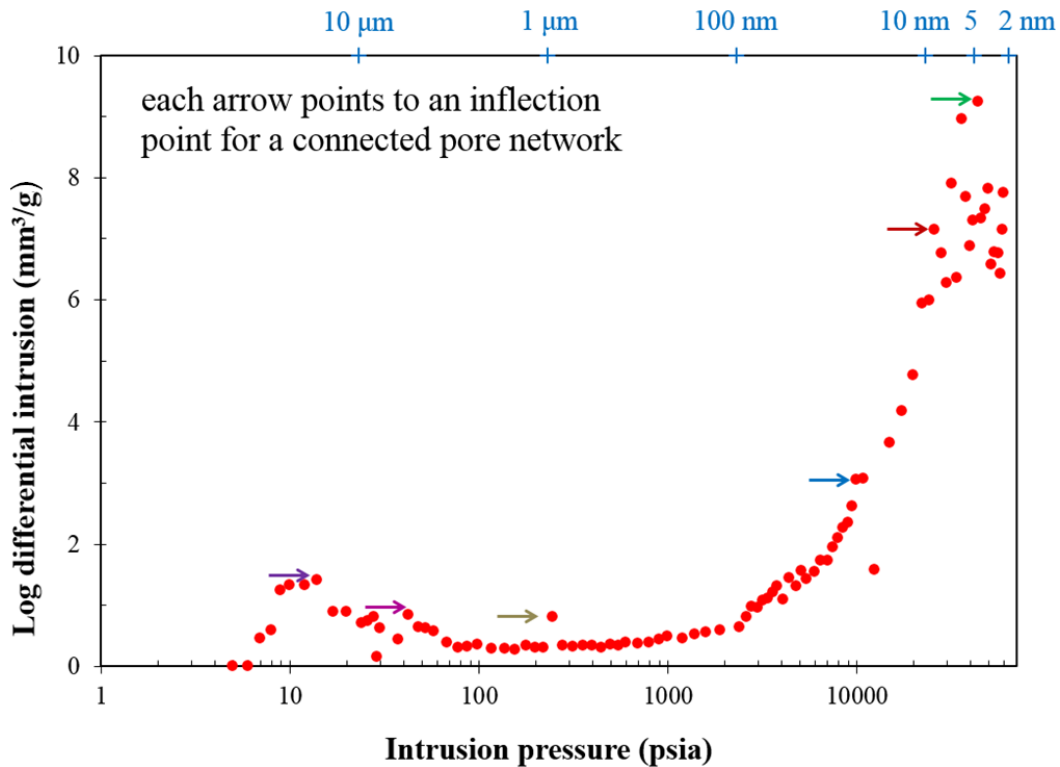


Figure 4-7 Log differential intrusion vs. intrusion pressure for sample A8829

The median pore-throat sizes for most samples range from 6.6 nm to 10.5 nm, while two samples, A8566 B and A8722, act as outliers due to the presence of fracture(s), with median pore-throat sizes of 20.9 nm and 27.0 nm respectively (Table 4-8). Six samples produce the highest volume of pores within the 0.005 – 0.01 μm pore-throat sizes, while two samples produce the highest volume of pores within the 0.01 – 0.05 μm and one within the 0.0028 – 0.005 μm range. All samples, except one (A8722) contain pore-throats smaller than 5 nm, probably related to organic matter and clays. Mercury intrusion did not detect pores with throats smaller than 5 nm for sample A8722. According to the classification of IUPAC (International Union of Pure and Applied Chemistry), the following pore size range is used for clays and shale rocks (Kuila and Prasad, 2012).

- Micropores: < 2 nm in diameter
- Mesopores: 2-50 nm in diameter
- Macropores : > 50 nm in diameter

The majority of pores present within the samples studied fall within the mesopore range with one sample, E6609, falling within the micropore scale.

Two samples within the dataset display the presence of fractures. A fracture is observed in the intrusion data at a pressure of 7.99 psia for sample A8566 B, and at a pressure of 6.99 psia for sample A8722. For such samples, we can specifically obtain fracture and matrix porosity, as well as pore-throat size distribution for the matrix. In A8566 B, the porosity was 3.09% with the fracture included and decreased to 1.1% with the fracture excluded from the data points. In A8722 the porosity was 1.96% with the fracture included, and decreased to 0.85% with the fracture excluded. The pore-throat size distribution is also affected by the fractures within the samples. For A8566 B, the majority of pores fell within the 10-50 μm range with the fracture included and fell to within the 0.005-0.01 μm range with it excluded. For A8722, the majority of pores fell within the 10-50 μm range with the fracture included and fell to within the 0.01-0.05 μm range with it excluded (Figure 4-8).

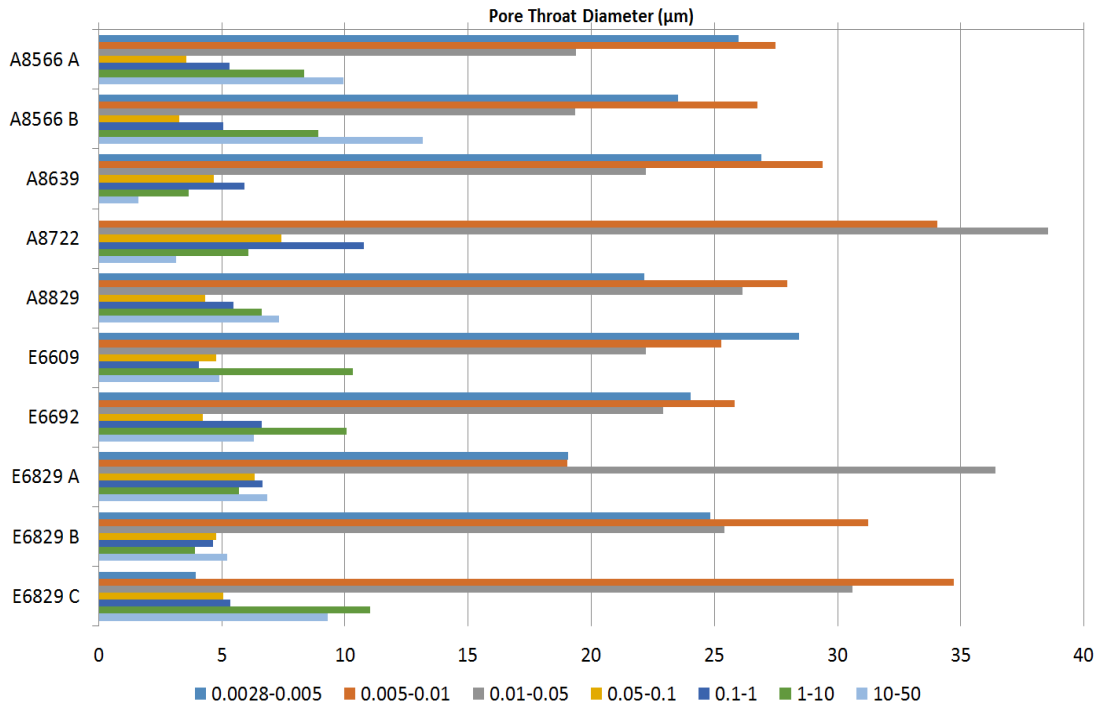


Figure 4-8 Graphical representation of pore-throat size distribution from MICP tests

Table 4-8 Pore characteristics obtained through MICP Analyses

Sample ID	Sample Mass Used (g)	Bulk Density (g/cm ³)	Total Pore Volume (cm ³ /g)	Total Pore Area (m ² /g)	Medium-pore-throat diameter (Area) (nm)	Medium-pore-throat diameter (4V/A) (nm)	Apparent (skeletal) density (g/cm ³)	Porosity (%)	Predominant Pore Network	
									Permeability k (mD)	Effective Tortuosity (Dimensionless)
A8566 A	2.50	2.42	0.005	2.8	4.3	7.8	2.45	1.3	1.44x10 ⁻⁶	3445
A8566 B	2.78	2.45	0.013	2.5	4.2	20.9	2.53	3.09	1.201 x10 ⁻⁶	19829
A8639	2.16	2.32	0.008	4.6	4.4	6.6	2.36	1.73	1.993 x10 ⁻⁶	1335
A8722	3.15	2.38	0.008	1.2	6.9	27	2.43	1.96	1.041 x10 ⁻⁵	5694
A8829	2.70	2.31	0.008	4.2	4.5	7.6	2.35	1.83	3.513 x10 ⁻⁶	2100
E6609	2.75	2.45	0.002	1.2	4.1	6.9	2.47	0.52	4.415 x10 ⁻⁷	3130
E6692	2.45	2.35	0.006	2.9	4.3	7.6	2.38	1.31	1.548 x10 ⁻⁶	2642
E6829 A	2.66	2.38	0.004	2.0	4.4	7	2.41	0.85	8.526 x10 ⁻⁷	3190
E6829 B	3.08	2.35	0.004	1.4	5.9	10.5	2.37	0.87	1.61 x10 ⁻⁶	3054
E6829 C	2.82	2.37	0.004	2.5	4.3	6.8	2.40	1.01	1.529 x10 ⁻⁵	829

4-4 Imbibition

In order to gain insight into the pore connectivity of the Woodford Shale for a specific fluid, spontaneous fluid imbibition tests were performed on seven samples using both DI water and n-decane. During the tests, fluid uptake was recorded by an analytical balance, and plotted on a log-log scale to obtain the imbibition slopes for each sample (Figure 4-9). Typically, imbibition behavior from the Woodford samples exhibits two slopes for n-decane imbibition, and three slopes for the imbibition of DI water. In a few instances, only two slopes were observed during DI water tests. The first slope (Region I) represents the settling of samples from initial surface contact with the imbibing fluid. The second slope (Region II) is representative of fluid migration across well-connected pores on the sample bottom and continuing up the exterior sides. The third slope (Region III) exhibits the fluid movement behavior in interior pores with a value of 0.5 or 0.25 to indicate the matrix pore connectivity. The fourth slope (Region IV), which is not always observed, levels out when the fluid reaches the top of the sample. For some n-decane tests this leveling out can be observed while no DI water test is conducted long enough, or not observable from its less wetted and poorly connected pores, to see this effect.

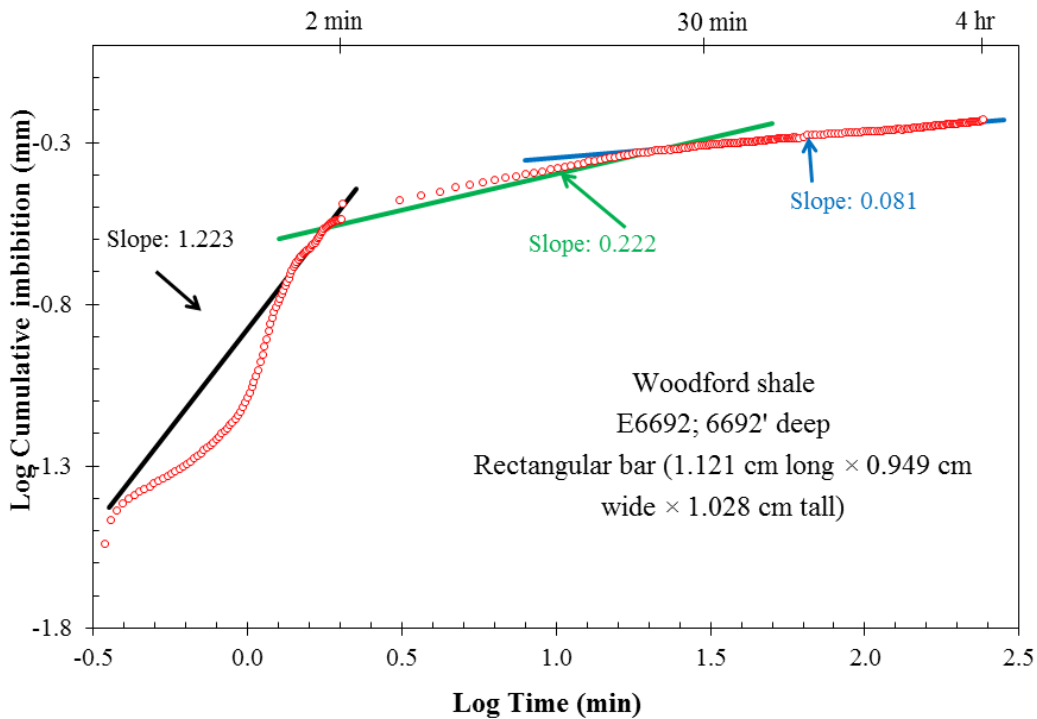
Fluid imbibition tests were first performed on three samples from Well E (Table 4-9). Both DI water and n-decane tests were run for a range of durations to identify the time period that provided the best results. After performing 24 hr DI water tests it was determined that by hour 12 the last slope had developed (Figure 4-9), so 12 hr tests were performed going forward. For n-decane, a four hour test (Figure 4-10) does not let the last slope develop enough so the test duration was extended to 6 hours moving forward; a slower imbibition time for n-decane to reach the sample top is related to its wetting behavior of these shales. The water imbibition tests provide low Region III slopes with an

average of 0.172 (Table 4-10). A low slope indicates low pore connectivity for a particular fluid, confirming the hydrophobic characteristics seen in earlier surface wettability tests.

Table 4-9 List of Imbibition Tests Performed.

Imbibition						
Sample ID	DI water (4 hr)	DI water (6 hr)	DI water (12 hr)	DI water (24 hr)	n-decane (4 hr)	n-decane (6 hr)
A8566	-	-	X	-	-	X
A8639	-	-	X	-	-	X
A8722	-	-	X	-	-	X
A8829	-	-	X	-	-	X
E6609	-	X	-	X	-	X
E6692	X	X	-	X	-	X
E6829	-	X	-	X	X	-

A)



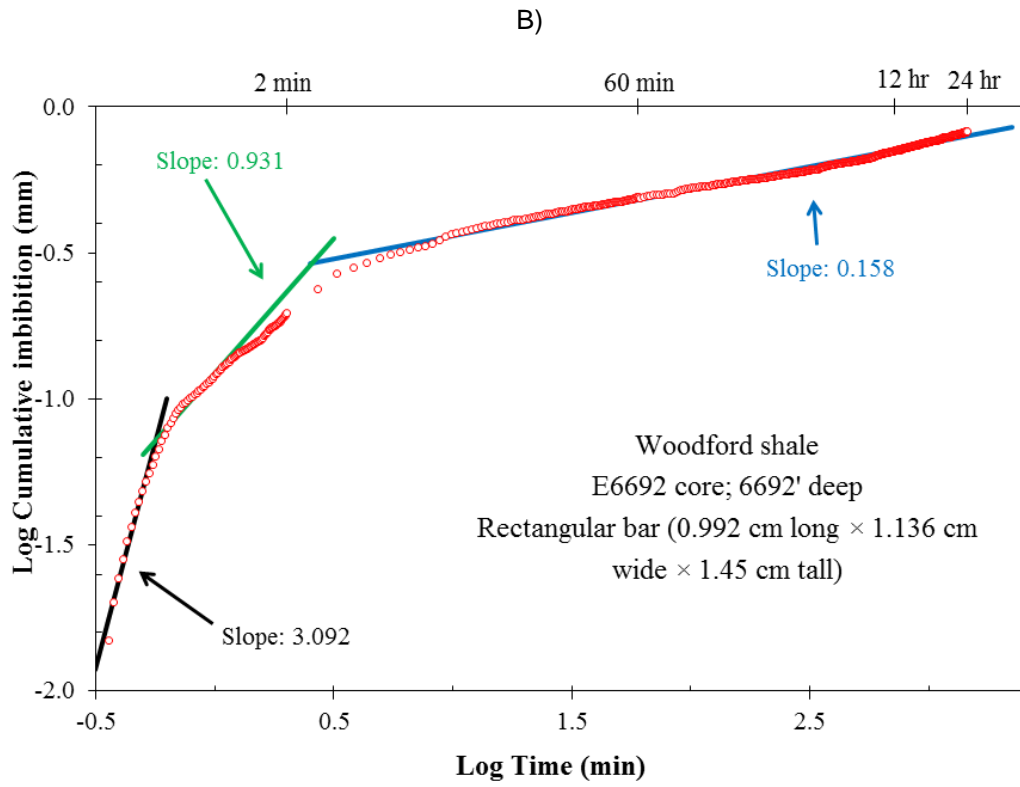


Figure 4-9 DI water imbibition into sample E6692 for A) 4 and B) 24 hours

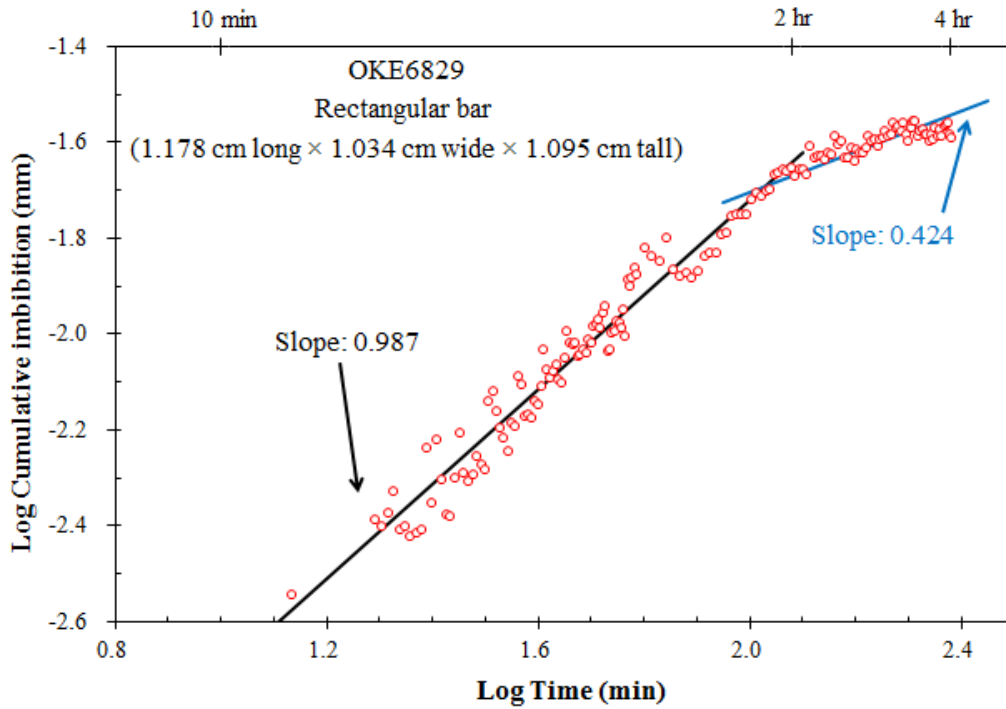


Figure 4-10 n-decane imbibition into sample E6829 for 4 hours

Table 4-10 Region III average slope for imbibition tests

Sample ID	Test	Region III Average Slope
A8566	n-decane	0.485
	DI water	0.128
A8639	n-decane	0.631
	DI water	0.181
A8722	n-decane	0.539
	DI water	0.081
A8829	n-decane	0.547
	DI water	0.125
E6609	n-decane	0.92
	DI water	0.323
E6692	n-decane	0.922
	DI water	0.126
E6829	n-decane	0.424
	DI water	0.177

N-decane imbibition tests provided much higher slopes in Region III than DI water (Table 4-10). Slopes averaged 0.558, indicating good pore connectivity with respect to oil wetting fluids, consistent with the wetting characteristics.

4-5 Log Analysis

Well log analyses were used to provide log-derived values for petro-physical properties such as porosity, permeability, and water saturation. While some logs can acquire data on a scale of a few inches, most provide an average reading over a few feet of rock (Barber, 1991). Laboratory tests run on core data, on the other hand, acquire data over sample sizes of mm-cm. Both are unique and should be considered when striving to understand the petro-physical characteristics of a reservoir. Because of the discrepancies between the scale of measurements, log data seem to always overestimate readings and it can be helpful to apply corrections based on the core data if available. Figures 4-11 and 4-12 below show the original log suites for Wells A and E with CORE_POROSITY, CORE_SW, LOG_SW, POR_MICP_UTA, DPLS_TOC_CORRECTION, and PERM_LOG. CORE_POROSITY is the porosity measured at Chesapeake and it is first plotted against the neutron-density porosity logs in Track 3. It is apparent that the density porosity curve overestimates the porosity and so a correction has to be made. This correction is shown as the DPLS_TOC_CORRECTION data points in Track 5, and a higher correlation can then be seen with the CORE_POROSITY curve. Also seen in Track 5 are the POR_MICP_UTA data points, achieved through MICP data processed on 7 shale samples. These values are even lower than those measured at Chesapeake indicating the variability within the rock and the inconsistency between measurement techniques and scales. In Track 4 two water saturation curves are visible. CORE_SW is based on core data measured at Chesapeake, while the LOG_SW curve was calculated using a modified Archie's Equation. Formation water resistivity in shales can be

extremely variable making it difficult to determine a fixed R_w value. The presence of large interconnected clays creates more paths for electrical current resulting in a reduction in formation and cementation factor (Rezaee, 2015). This causes the water saturation calculated by Archie's equation to be over-estimated and not a direct measurement, but for quick analysis of intervals it will suffice. Mazaheri et al. (2015) discusses the volume influence of neutron, density, gamma ray and resistivity logs stating that fractures can throw off these readings considerably as well.

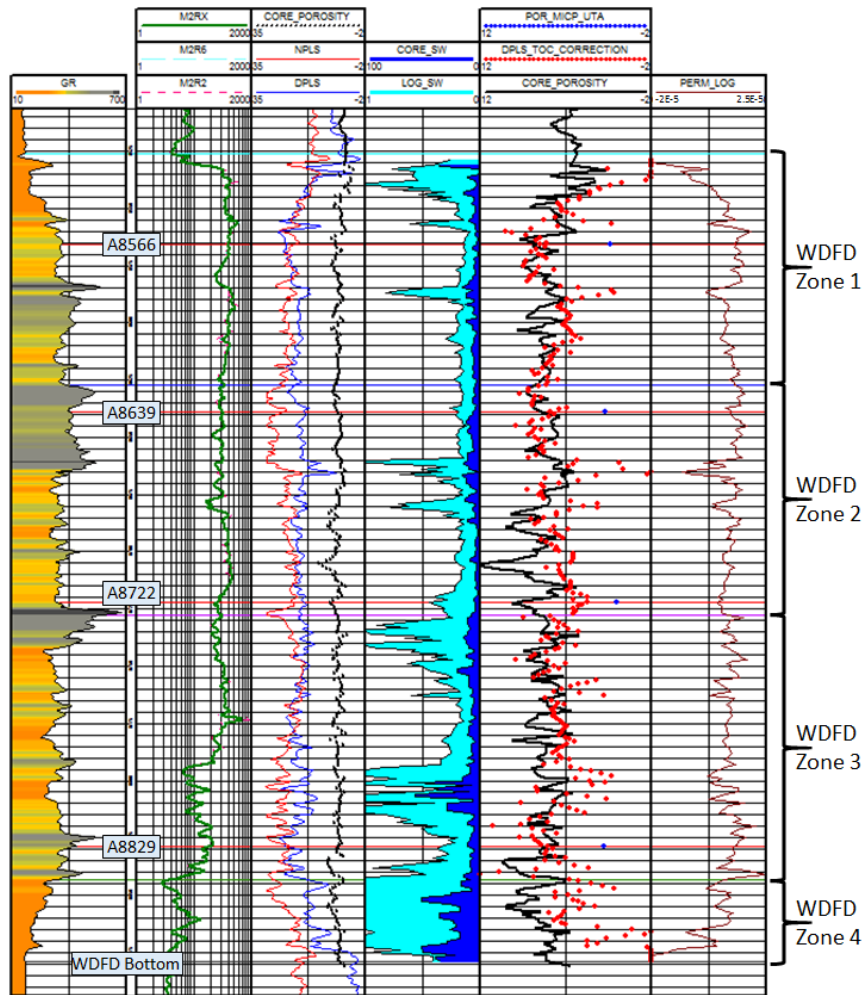


Figure 4-11 Log Analyses of Well A

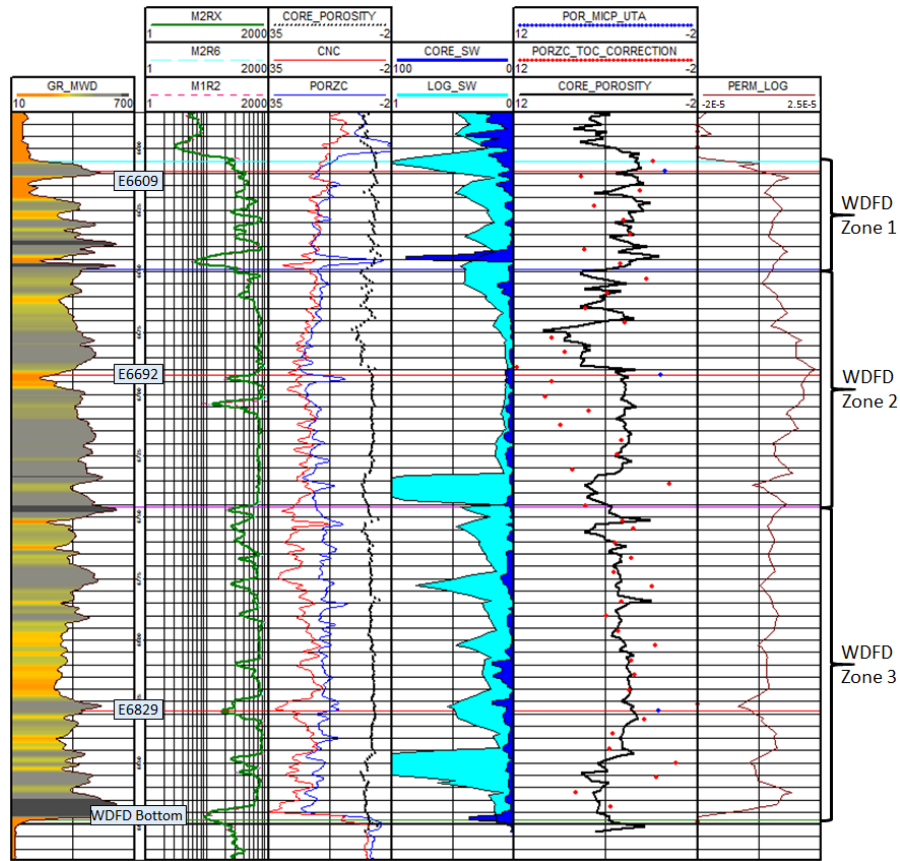


Figure 4-12 Log Analyses of Well E

4-6 Porosity and Permeability from Different Approaches

Porosity and permeability values for samples used in this study were obtained using three different techniques. MICP analyses provide both permeability and porosity values as well as a relationship between the two that was further used with well logs to calculate a log based permeability. Density porosity logs provide porosity measurements that are then corrected using a TOC cutoff and differing matrix densities. Core porosity and permeability values obtained by Chesapeake are also taken into account. Results are shown in [Tables 4-11 and 4-12](#) as well as [Figures 4-13 and 4-14](#).

Table 4-11 Porosity Results from Various Approaches

Sample	Depth (ft)	MICP (%)	Chesapeake Core (%)	Density Log (%)	
				Original	TOC Correction
A8566 Ave.	8566	1.2	7.91	23.55	7.03
A8639	8639	1.73	6.61	17.71	6.19
A8722	8722	0.85	9.39	17.92	3.2
A8829	8829	1.83	7.22	23.42	6.49
E6609	6609	0.52	4.2	20.16	6.86
E6692	6692	1.31	3.3	21.07	9.13
E6829 Ave.	6829	0.9	2.7	16.56	2.09

Table 4-12 Permeability Results from Various Approaches

Sample	RTC GRI (mD)	MICP Perm. of Pore Size with greatest volume % k (mD)	MICP Geometric Mean k (mD)	Log Permeability (mD)
A8566	1.42×10^{-4}	1.32×10^{-6}	4.92×10^{-9}	1.4×10^{-5}
A8639	1.59×10^{-4}	1.99×10^{-6}	8.52×10^{-10}	1.2×10^{-5}
A8722	2.38×10^{-4}	1.04×10^{-5}	2.4×10^{-9}	6×10^{-6}
A8829	1.32×10^{-4}	3.51×10^{-6}	3.29×10^{-9}	1.2×10^{-5}
E6609	4.77×10^{-4}	4.41×10^{-7}	1.38×10^{-9}	2×10^{-6}
E6692	1.09×10^{-3}	1.55×10^{-6}	1.36×10^{-9}	2×10^{-5}
E6829	7.17×10^{-4}	5.92×10^{-6}	9.69×10^{-5}	1×10^{-6}

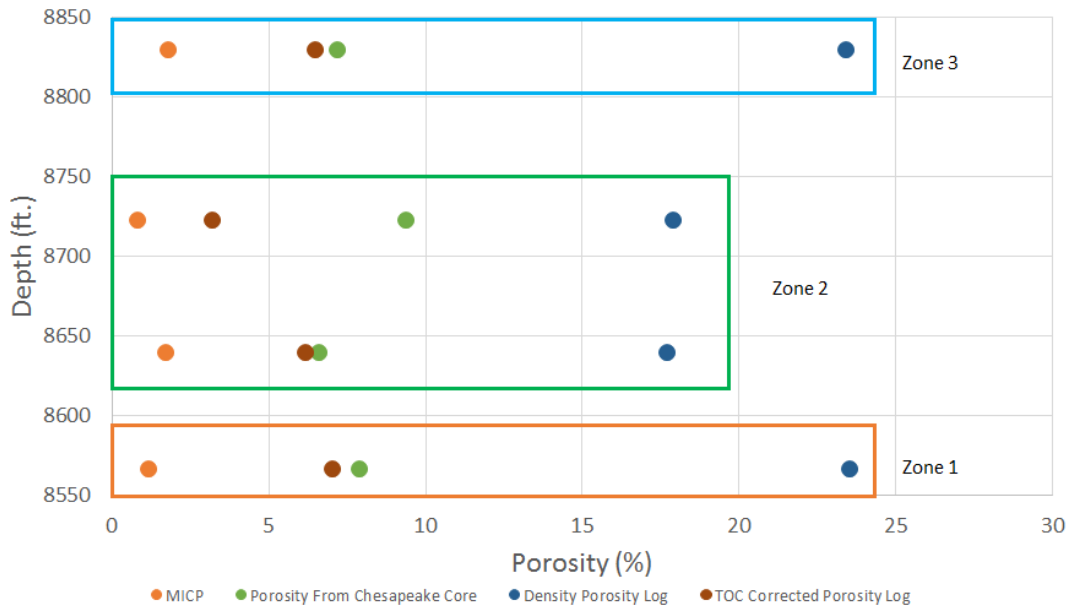


Figure 4-13 Porosity cross plot for Well A

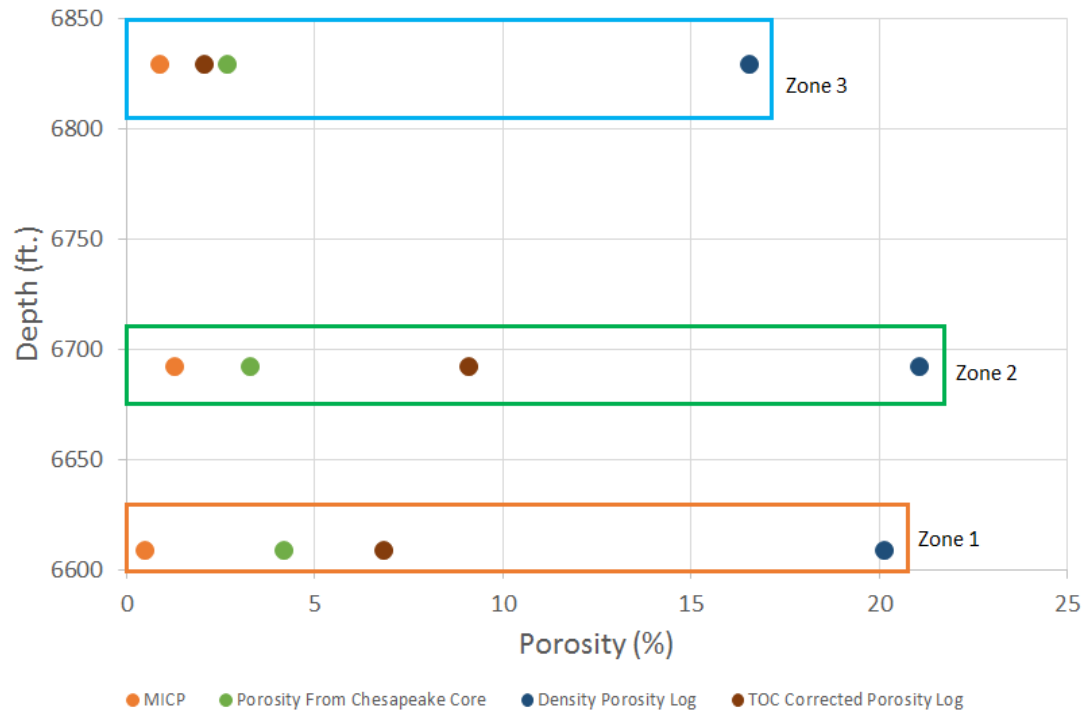


Figure 4-14 Porosity cross plot for Well E

4-7 Production Data

Well A began its production on October 29th, 2008 as a horizontal well in Woodford Shale, with an initial production of 70 barrels per day (bbl/day) and 950 Mcf of gas a day. Cumulative production from Well A is 33,522 bbl and 765,669 Mcf of gas, and the well is still online (Figure 4-15). Well E began production as a horizontal well on February 26th, 2012 with 173 barrels per day (bbl/day) and 1,775 Mcf of gas. Cumulative production has reached 25,549 bbl and 579,082 Mcf and the well is still online (Figure 4-16). Data summarized below in Table 4-13 and Figures 4-15 and 4-16. Both wells have been producing both oil and gas.

Table 4-13 Completion details for study wells

	Well A	Well E
Completion Year	2008	2012
Measured Depth (ft)	13,750	11,531
True Vertical Depth (ft)	8,708	6,679
Lateral Length (ft)	8,650 – 13,750 md	6,675 – 11,427 md
Perforation Interval (ft)	3	-
Cumulative Oil (bbl)	33,522	25,549
Cumulative Gas (Mcf)	765,669	579,082

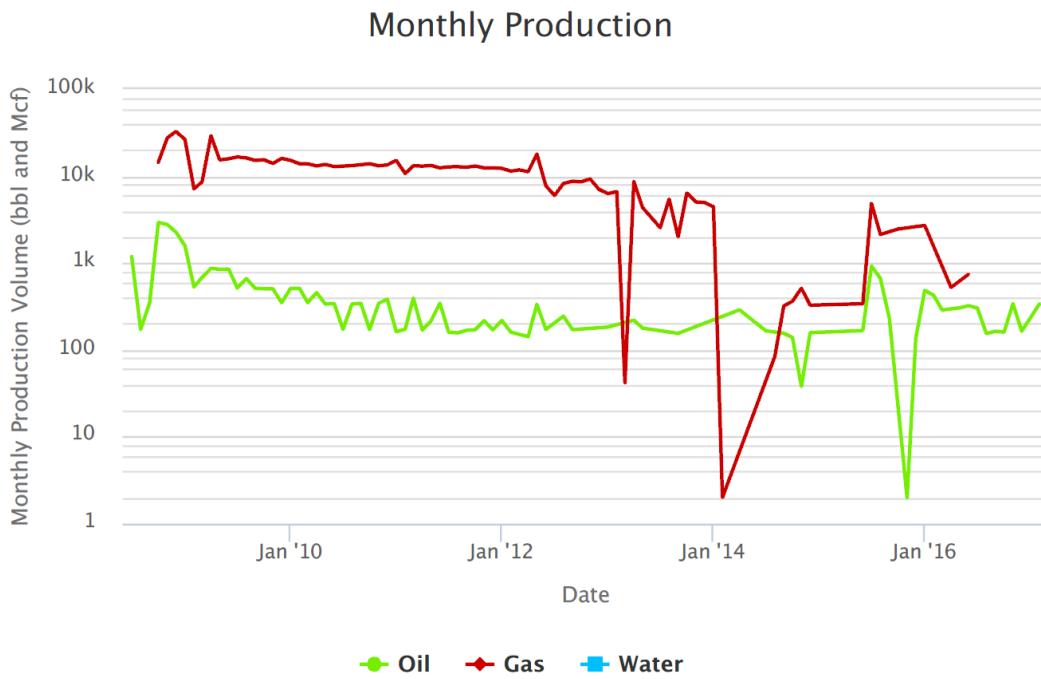


Figure 4-15 Monthly Production over Time for Well A from DrillingInfo (the company declines to provide daily production/pressure data, as well as any operation factors related to production bumps).

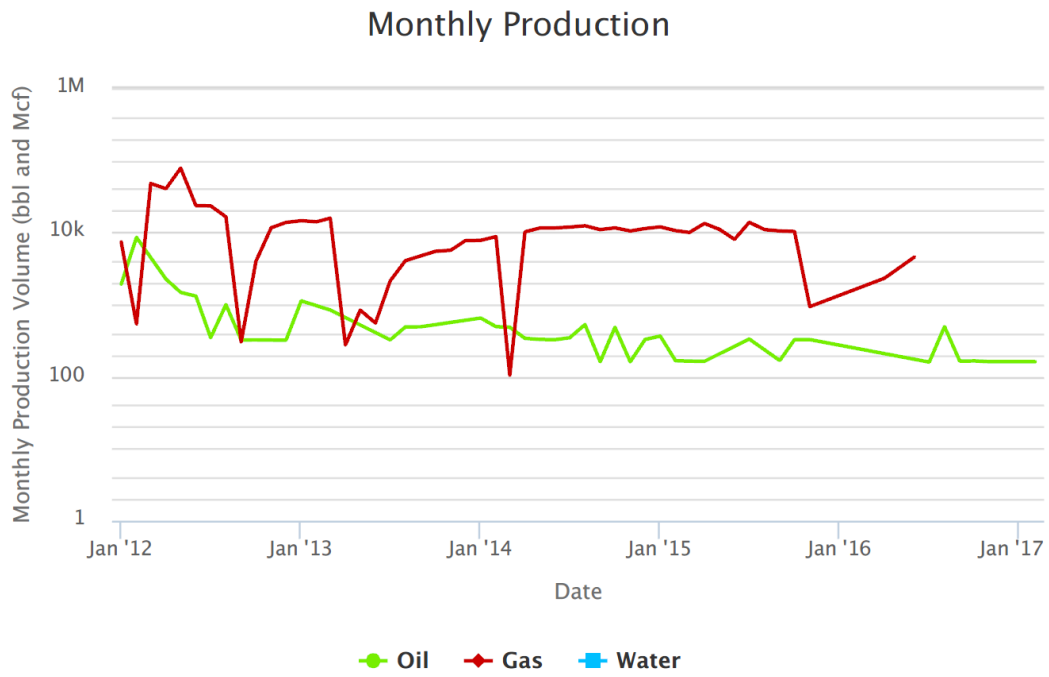


Figure 4-16 Monthly Production over Time for Well E

Chapter 5 Discussion

5-1 Mineralogy and Geochemistry

As discussed, the Woodford Shale is composed of interbedded organic-rich shale and chert. Zones 1 and 2 in both wells contain a very small amount of clay minerals while Zone 3 is relatively high in clay contents. There is no correlation between TOC and clay or quartz contents (Figure 5-1), indicating a complex inter- and intra-granular pore structure that cannot be explained by a single metric. This contradicts the findings of Gupta (2013) that a trend of increasing TOC values exists with increasing quartz content. The discrepancy most likely exists due to the small sample of this thesis compared to the 300 samples analyzed by Gupta (2013). A trend would likely present itself if more samples were studied.

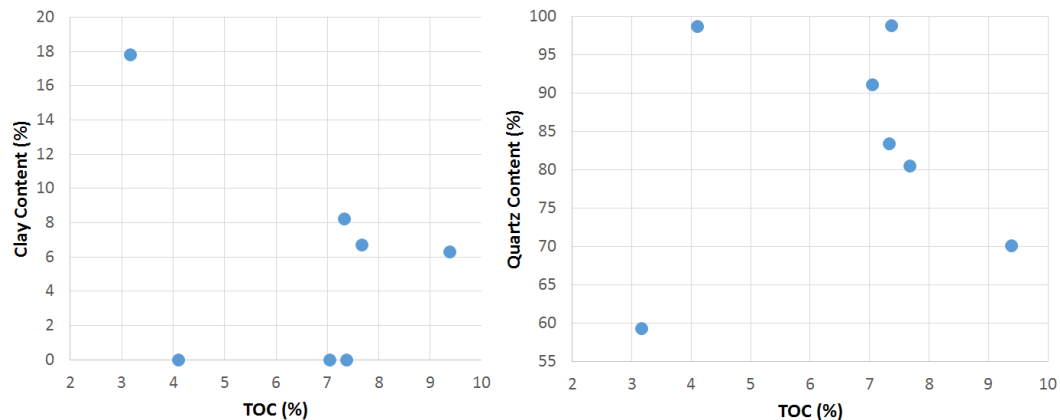


Figure 5-1 Mineral percentages vs. TOC

When porosity values obtained through MICP are plotted against quartz percentages, a negative correlation can be seen as compared to a positive correlation between porosity and clay percentages (Figures 5-2 and 5-3). The same positive clay/porosity correlation is seen in a Woodford sample set of 300, studied by Gupta (2013), while no particular correlation was seen between quartz and porosity in the same study (likely due to sample

set size). This can be explained by the fact that organic matter-hosted pores are considered the dominant contributors to total porosity in organic-rich unconventional reservoirs, and are also closely associated with clay minerals (Lohr et al, 2015). The relationship between clay minerals and organic matter hosted pores would indicate that Zone 3 would be the ideal zone to encounter the greatest porosities even though this trend was not seen in the overall porosity measurements previously discussed. In addition, there is no clear correlation between permeability and mineralogy.

Pyrolysis data do not suggest many distinctions between the zones within the Woodford Shale with regards to hydrocarbon generation or kerogen type. The whole section is under mature, oil and gas producing, but gas prone, with type II/III kerogen. One distinction that can be made is the small amount of crossover between TOC and S1 that occurs in Zones 2 and 3 in Well E indicating hydrocarbon generation. This would be an ideal section to target considering the potential of producing oil as well as gas.

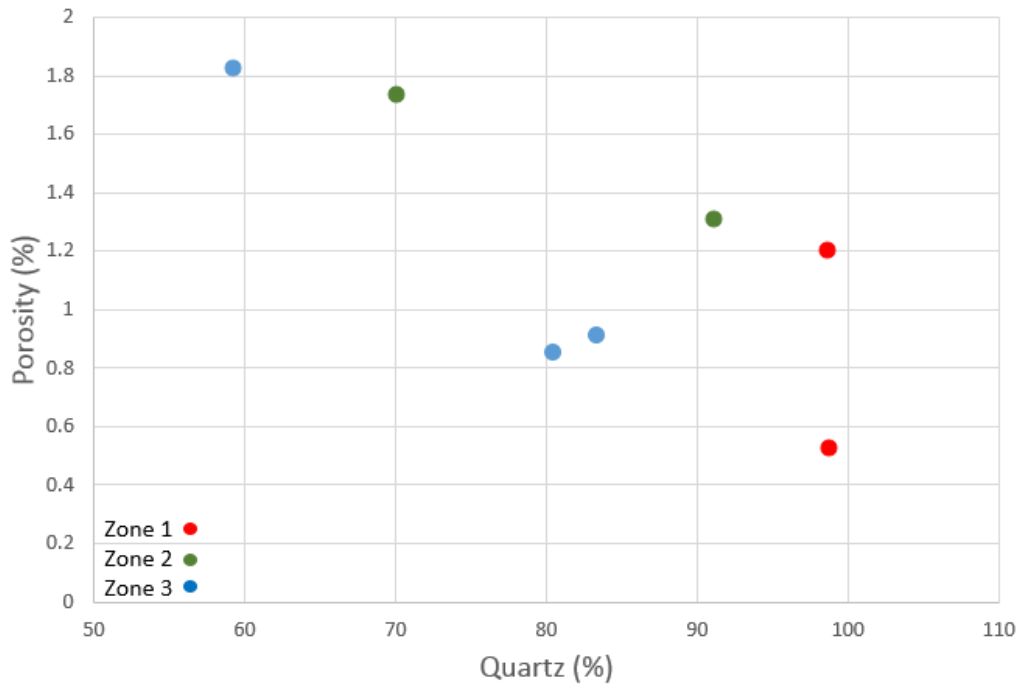


Figure 5-2 Quartz vs. Porosity

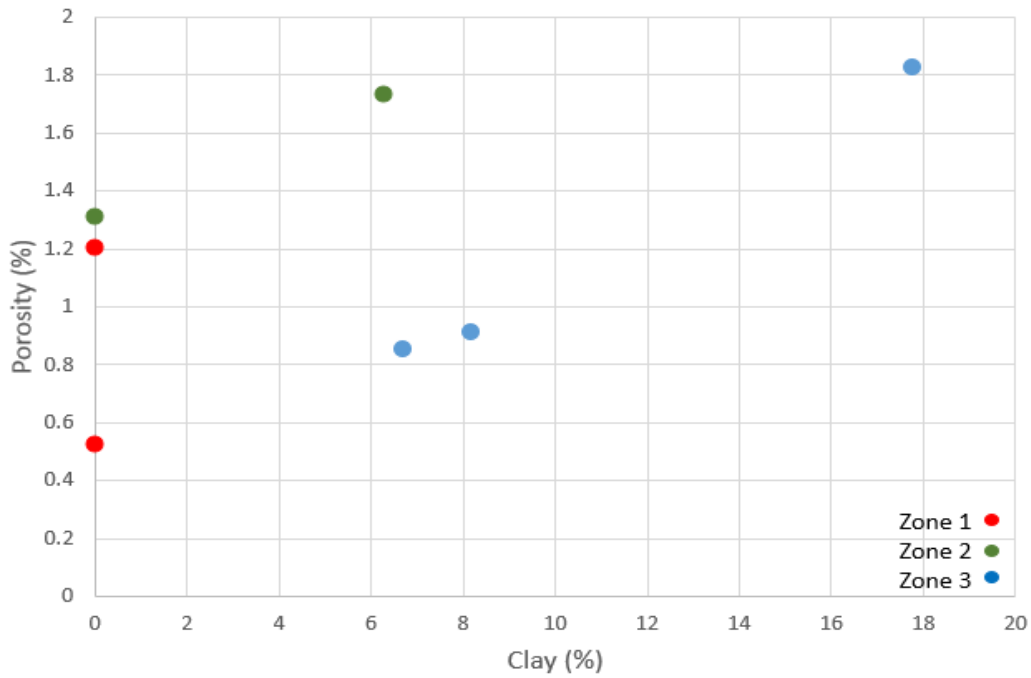


Figure 5-3 Clay vs. Porosity

5-2 Wettability

Both wettability tests performed for this research portray a strong oil-wetting behavior for the Woodford samples. This observed hydrophobic behavior describes the natural tendency of the pores in each sample to be filled with oil over water. Now this is not a direct indication that the samples are occupied by oil, but if both oil and water are introduced to the reservoir, the oil is more likely to be trapped in pore space while the water will be repelled. Water saturation log analysis helps to indicate sections of reservoir that are more heavily occupied by water and when coupled with wettability results predictions can be made for when highly saturated sections will be encountered in future boreholes. The use of four different fluids (DI water, API brine, 10% or 20% IPA and n-decane) helps to display the spectrum of wettability for each sample. Both the qualitative and quantitative assessment of wettability characteristics show the lowest affinity to DI water, then API brine, 10/20% IPA and lastly n-decane, except for samples A8722 and A8829. These inconsistencies are possibly due to a change in mineral composition, most likely an increase in clay content for a higher affinity to DI water.

5-3 Pore Structure Characteristics from MICP Analysis

MICP data allow the pore structure of the top three Woodford zones to be characterized and compared. The bulk densities for each well correlate nicely to their respective zones. Zone 1 in both wells has a bulk density of 2.45 g/cm³, while Zone 2 has bulk densities of 2.38 and 2.36 g/cm³, and Zone 3 with densities of 2.40 and 2.43 g/cm³. Bulk density is important to note as it indicates the kerogen content of the sample because of the low grain density of organic matter. Zone 2 has the lowest bulk density readings, suggesting a higher TOC value and more oil-rich zone (Passey et. al., 2010). This assumption is also evidenced by the largest TOC values in Well A coming from Zone 2. Gupta et al (2013) studied Woodford samples from six wells in midwest

Oklahoma and found a density range of 2.2 to 2.9 g/cm³, which encompasses the densities measured in this study. The medium pore-throat diameter decrease with depths with Zone 3 having diameters close to 6 nm. Gao and Hu (2013) developed a relationship between the median pore-throat radius and permeability stating that most other parameters have a negligible effect on permeability. This is seen in the data as there is a strong correlation (~93%) between permeability and porosity measurements. Zone 3 has the largest pore-throat diameters and if considering Gao and Hu's relationship, the highest permeability values as well. Porosity measurements do not present a pattern with respect to certain zones, but there are positive correlations with pore volume, area, and pore-throat diameter. Based on the pore structure data acquired, Zone 3 would provide the highest rate of fluid flow into the borehole.

5-4 Pore Connectivity

The slopes acquired through fluid imbibition tests relate to the pore connectivity of each sample and provide insight in the most well-connected zones within the Woodford Shale. Since the Woodford Shale is an oil and gas producing reservoir, the focus will be on the slopes provided by n-decane tests. Region III indicates the fluid interaction with interior pores and levels out when the fluid reaches the top of the sample. The slope corresponding to Region III in Zone 1 samples is 0.485 in Well A and 0.92 in Well E. The range in this zone provides no correlation and further testing would have to be done to draw any conclusions for Zone 1. In Zone 2, both wells provide slopes above 0.5 indicating good connectivity throughout the interior pores. Well A has a Zone 3 slope above 0.5 while Well E has a Zone 3 slope below 0.5 indicating no correlation between the two. Based on pore connectivity alone Zone 2 would provide the best connected pore network for fluid flow.

5-5 Porosity and Permeability

Porosity and permeability have traditionally been the benchmarks for deciding whether or not a formation may produce oil and gas. With the development of fracture networks through fracturing techniques, permeability has become less important for a well to be an economic success, but understanding the fluid flow through absolute permeability allows for a better picture of reservoir drainage. Porosity is still highly important but it has become more difficult to quantify accessible porosity due to organic matter (OM)-hosted pore spaces which are relatively isolated from surrounding mineral pores. It is difficult to quantify OM hosted porosity without performing SEM analyses to image pore type, but a positive correlation between TOC and porosity would indicate OM hosted porosity. **Figure 5-4** below shows no particular trend line which is an unexpected result, because **Gupta et al (2015)** found a positive correlation with three hundred samples. The positive correlation might not be seen here because of the limited number of samples. As seen in **Figures 4-11 and 4-12**, four different porosity measurement techniques provide a range of values from 0.5 to 23%. This includes density porosity log measurements which regularly overestimate porosity values. Taking these values out provides a much more reasonable range of 0.5 to 9.1% that correlates well with the porosity range of 0 to 10% found by **(Gupta et al, 2013)**. In Well A, there it is not clear which zone provides the highest overall porosity but when only taking the Chesapeake core values into account Zone 3 provides the highest measurement. In Well E, Zone 2 provides the highest range of porosities. Permeabilities are shown in **Figure 5-5** and range from 4.41×10^{-7} mD to 2.16 mD. High, dominant, and low MICP permeability correlate with the respective pore-throat diameters. Dominant MICP results as well as log permeability measurements indicate the most realistic permeabilities based on the highest occurring pore throats. Zone 3 provides the highest permeability range.

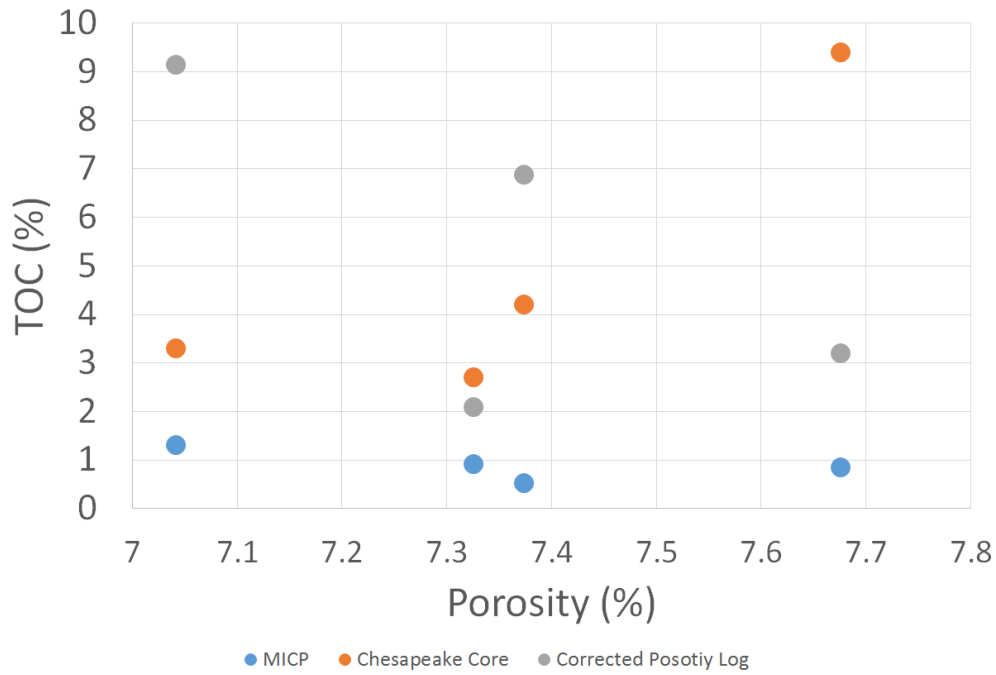


Figure 5-4 Porosity vs. TOC

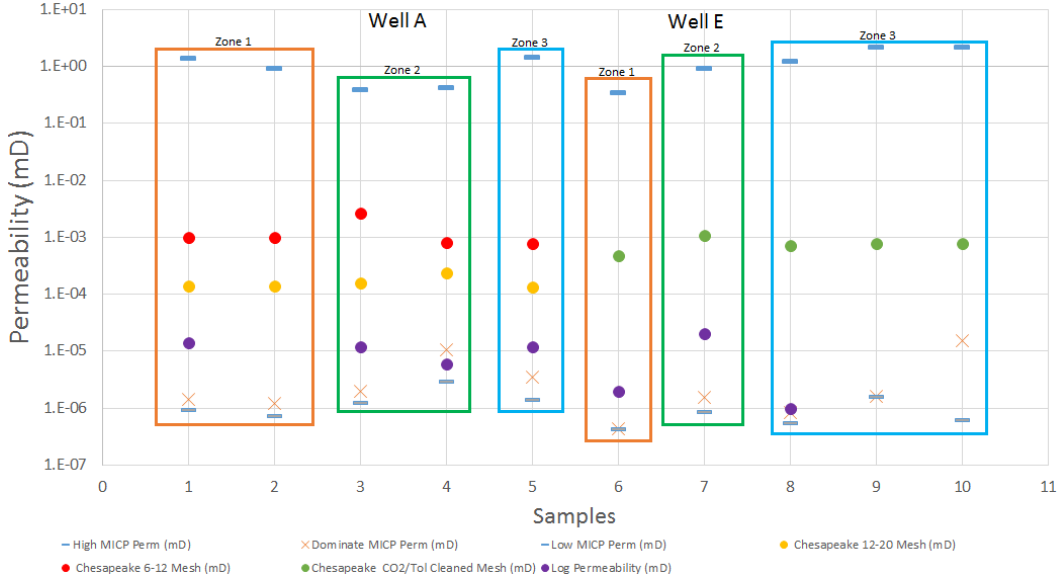


Figure 5-5 Comparison of Permeability Values from Various Techniques

5-6 Well Logging and Producibility

Horizontal Woodford Shale wells drilled in the Ardmore Basin will almost surely produce hydrocarbons, but for these wells to be economical the wellbore must be placed in the zone containing the ideal petro-physical characteristics for drilling as well as production. In Well A, Zone 1 is 50' thicker and gives a relatively low gamma ray reading representative of less organic material and more sandstone, siltstone or dolomites. In Well E, both high and relatively low gamma ray signatures occur, indicating interbedded shales, siltstones, sandstones, and a heterogeneity that might make it difficult to predict the reactions of a drill bit moving through this zone. In both wells neutron-density logs come together and cross, more than in any other zone indicating the possibility of gas content. The smallest porosities in both wells are encountered in the first 50' of Zone 1 and permeabilities cover the range of values encountered, increasing with depth. Water saturation is high at the top of the section but decreases with depth.

Zone 2 in both wells has the same thickness, consistently high gamma ray readings of organic pelagic shales, and low water saturation except for a few highly saturated thin sections. Porosity values are higher in Well A and take a dip in Well E throughout the second half of the zone. Neutron-density crossplots remain close rarely crossing through Zone 2. Permeability measurements hit a high point some 50 feet into the interval. Zone 3 is highly saturated with water in both wells compared to other zones, and produces average porosity and permeability values. The neutron-density crossplot curves tend to separate suggesting a less gas prone zone. Zone 2 looks to be the ideal zone to place a borehole in, based on the thickness, low water saturation, and neutron-density porosity.

Chapter 6 Conclusions and Recommendations

6-1 Conclusions

The purpose of this study is to investigate the petro-physical characteristics of different zones within the Woodford Shale in the Ardmore Basin while also commenting on the necessity for standardized tight rock laboratory tests. Porosity and permeability measurements obtained by different parties range from 0.5 to 9.4 % and from 4.41×10^{-7} to 2.64×10^{-3} respectively, both outside the typical margins for error. The differing results speak to the heterogeneity of the rock and sample sizes used in the analyses, but the difficulty in the quantitative analysis of said characteristics is evident in the oil and gas industry's inability to develop a standard suite of tests for shale like the ones that exists for conventional reservoir rock. Without a standard, separate laboratories often provide differing characteristics from the same reservoir rock adding to the inability to comprehensively understand the factors affecting shale oil and gas production. Further research is needed in order to develop reproducible workflows for measuring shale rock characteristics as well as to identify patterns between these characteristics and current production methods.

The samples chosen are of different lithologies and TOC contents in an effort to summarize the properties of a roughly 300 foot section of the Woodford Shale. In both wells the wettability of the rock shows hydrophobic tendencies. The pore structure of all samples lends itself to potentially organic (5-10 nm) or intragranular (5 – 50 nm) pore-throat sizes with Zone 2 containing the highest bulk densities. Fluid imbibition describes the samples as containing high pore connectivity for hydrocarbons with Zone 2 presenting the most well-connected pore networks. The highest porosity values are found in Zone 3 for Well A and Zone 2 for Well E, while Zone 2 contains the highest

permeability values for both wells. Quartz makes up most of the samples' mineralogy with six samples being described as a silica dominated lithotype and one as a clay-rich siliceous mudstone. There is a relatively strong correlation between clay content and increased porosity suggesting the interval with the highest clay contents, Zone 3, also contains higher porosities. Based on well logs measurements of the full Woodford section as well as historical production and wellbore placement, Zone 2 looks ideal for hydrocarbon production if the interval of high water saturation and low permeability values in the middle of the zone is avoided. Overall Zone 2 contains the best petro-physical properties for a likely successful well within the Woodford Shale.

6-2 Recommendations

The relationships found in this work are only relevant for the small amount of each sample examined in this thesis and the limited sample size may prevent the results from being quantitatively applicable at a larger scale. To improve on these results, more samples must be investigated to create a comprehensive data set and lend confidence in the conclusions made. SEM imaging is needed to provide pore type information to supplement volumetric results of multiple connected pore networks from MICP analysis. The petro-physical properties measured on carefully collected samples indicate the importance of TOC, porosity, quartz and clay contents for identifying different rock types within the Woodford Shale and a continued look into the relationships between TOC content, porosity, permeability, pore network, and fluid flow mechanisms, and is necessary to achieve sustained producibility from this formation.

Appendix A

XRD Standard Operating Procedure

MaximaX XRD-7000: Shimadzu X-ray Diffractometer

Sample Preparation

- Prepare your sample by compacting the sample into the sample holder using a glass slide
- Avoid vertical loading by removing excess sample with the edge of the glass slide
- Attempt to make your sample as flat and homogenous as possible; once this is completed your sample is ready to be analyzed.

Power Operations

- Turn the chiller on by pressing the power button (on the face of the chiller), a green light will illuminate.
 - Allow the chiller to sit for ~20 minutes to adjust to the proper temperature.
- Turn the XRD on by pressing the power button on the left hand side. The green power button will illuminate on the front panel of the XRD.

XRD Calibration:

- Locate and open the [PCXRD] program on the desktop. The main "XRD-6100/7000" panel will display.
- Click the [Display and Setup] icon, a "door alarm check" window will pop up. Follow the prompt to open and close the XRD door, once complete click "Close". An "IOcon" window will pop up with the message "Now Calibration! If ready OK", Click "OK".
- The XRD is officially calibrated and ready to process your sample.

Setting Analysis Conditions:

- To set the processing conditions go to the "XRD 6100/7000" panel.
- Click on the [Right Gonio Condition] icon to open the [Analysis Condition Edit Program] window
- Click the blue bar under [Measurement Mode: Standard] to open the [Standard Condition Edit] window.
- Most of the settings in the [Standard Condition Edit] window will be preset. Only a few conditions will need to be changed.
- The following general condition settings will work for a wide array of materials.
It's very important to follow these next steps, double check any settings you change ensuring to follow these guidelines precisely. This will minimize minor mistakes when processing materials and will prevent damage to the detector.
 - Scanning condition: Scan Range (deg) = 2°-70° Optional Condition: Check the box [Option Enable]
 - Beta Attachment: Control Mode: Rotation
Rotation Speed (rpm): 6
 - Slit Condition: Slit Conditions are preset, and must be verified on the XRD to ensure the proper slit sizes match the settings listed under the Slit Conditions.
 - Checking the Slits:

- Open the XRD door, on the left side of the XRD is the X-ray tube, the Divergence Slit is attached to the left side of the divergence sollar slits.
 - On the right hand side will be the detector arm which contains a set of Scattering sollar slits, the Scattering Slit faces the sample (Left) and the Receiving Slit faces the detector (Right).
 - If they are not the same sizes as what is preset in the [Slit Condition] box change the slit's so they do match.
 - Standard Slit Settings:
 - Divergence Slit: 1.0°
 - Scattering Slit: 1.0°
 - Receiving Slit: 0.3 mm
- Double check your settings and make sure they are correct, if they are click [OK].
- A [File & Sample Condition Edit] window will display; change the [Group name] to match your destination folder name and change [File name] and [Sample Name] to match your sample name, click [New].
 - Later samples can be created by simply changing the file and sample names and clicking [Modify].
- Click [Close] on the [Standard Condition Edit] window.

Starting the XRD Processing:

- Locate and click the [Right Giono Analysis] icon on the [XRD-6100/7000] panel.
- Your current sample name should appear highlighted blue in the upper portion of the [Right Gonio System: AnalysisCondition Edit Program] window. Highlight your sample and click [Append], this adds your sample to the list in the bottom portion of the window labeled [Entry for Analysis], click [Start]. Your sample should appear in the bottom of the [Right Giono Analysis & Spooler Program] window, click [Start] in this window. This officially starts the analysis process.
 - Indicators for Analysis: A clicking sound will come from the XRD when the locking mechanism on sliding door locks. On the face of the XRD a yellow light should illuminate under [X-RAYS ON].
- Leave all software windows open and allow the XRD to process your sample, this should take ~30 minutes.

Completed XRD Processing:

- A complete peak spectrum should appear in the [Right Giono Analysis & Spooler Program] window upon completion.
- The green [Analyzing!] Box should disappear and the yellow [X-RAYS ON] light should turn off.
- If you have more samples to analyze, continue to run your samples in the same manner listed above.

Opening Peak Profile Spectrum:

- Locate and open the icon for the [MDI jade 9] software on the Desktop.
- Under [file], click [Read], locate the folder [xddat] under [favorites]. Locate the folder where your samples are saved.
- In your folder, each sample should have a [.RAW] file, use this file to open your selected spectrum in the [Jade 9] software.

Identifying Minerals in Peak Spectrum:

It's important to have an educated background on the sample you're analyzing. Knowledge regarding the bulk composition and what you're searching for will greatly reduce the amount of time spent IDing the various peaks in the spectrum.

- Locate the [Find Peaks] icon on the main tool bar next to the [Floppy Disk/Save] icon, this will identify and mark any statistically significant peaks within the spectrum
- Choose a mineral database: At the top of the panel to the right of the spectrum window, there will be a drop down menu choose the [RDB-Minerals] as the database. The RDB-Mineral database should be predominately used to identify most minerals in your spectra.
 - If you cannot find a mineral in the RDB-Minerals database change to the [PDF+4 Minerals] database library, but be sure to change back to the RDB database once the mineral is located.
- Begin searching for minerals based on your pre-existing knowledge regarding the sample. When you identify minerals that fit your peak spectrum hit [Enter] on the keyboard, this process will add the minerals to a compiled list of those minerals which you identified in the spectrum.
- Once you have exhausted your initial hypothetical list of minerals, a helpful tool to use is the [Line Based Search/Match]. Go to the main tool bar and locate [Identify] and select the [Line Based Search] option.
 - This tool will compile a list of minerals by searching a selected PDF database for entries with peaks which are statistical matches for the peaks identified within your spectrum.
 - Settings:
 - [Two-Theta Error Window] max setting should be no more than 0.24%
 - [Top Hits to List] max setting 80
 - Set the parameters and click the blue [Play] icon next to the [X] to run the search and generate a list of possible phases that might fit your spectra. *Note: the line based search should not be used as a primary way to identify the bulk mineral mode of the sample as the software is not consistent when generating phases and will possibly leave out important phases for the spectrum*.

Model Analysis:

- Once all minerals have been ID'd, check that they have been added to the mineral list by pushing [Enter] on the keyboard.
- Click the [%] icon next to the drop-down mineral list located on the toolbar in the middle of the window to begin modal analysis.
 - An overlay will appear with different chart configurations of the modal results, to change the configurations of the chart use the drop down menu in the chart window.
- To view the modal analysis in text format: locate and click the [...] icon near the [%] icon. This will list the minerals by name, chemical formula, and the normalized weight percent for each mineral. It will also state if the mineral is a [major], [minor], [trace], or [absent] component in the sample.
- If you would like to remove a mineral from your mineral list at any time, highlight the mineral and press [Delete] on the keyboard. [Absent] phases should be removed from the list by this method.

Analysis Check with Pattern Deconvolution:

- A key indication that the peak spectrum has been fully fitted and identified is by using the [Pattern Deconvolution] tool which automatically runs with the modal analysis.
 - The pattern deconvolution tool will generate a red overlay spectrum on top of the original white spectrum.

- This process is generating a [Best Fit Profile] composed of the selected mineral standards from the [Mineral PDF database library] with your sample spectrum.
- If all minerals have been properly identified, then the red deconvolution overlay will match the peak spectra for each peak. If there are peaks that don't have the red deconvolution overlay then those peaks have not been identified.
- Continue processing your spectrum until your original spectra and the deconvolution spectra match.

Saving Data:

To save your data,

- Go to [file] and [Save], save your data under [Current work as *.SAV]. This will save all analysis as a separate file.

Appendix B

TOC Standard Operating Procedure

Shimadzu TOC-V_{ws} SSM-5000A

The SSM-5000A is a solid sample module which can run two types of analysis, Total Carbon (TC) and Inorganic Carbon (IC), both of which are analyzed by a nondispersive infrared detector (NDIR). By subtracting the IC values from TC values, the Total Organic Carbon (TOC) of a sample can be quantified.

Methods

The TC method

- Uses the electric furnace to heat the combustion tube to 900°C, this allows the carbon combustion oxidation reaction to occur and will yield carbon dioxide which will be analyzed through the NDIR.

The IC method

- Uses the electric furnace to heat the combustion tube to 300°C, and, by adding 0.4 mL of 33% Phosphoric Acid (H₃PO₄), for the carbonate acidification reaction to occur, will yield carbon dioxide which will be analyzed through the NDIR.

Sample Table

- a. Open [TOC-V Sample Table Editor] icon and enter your initials
- b. Click the [New] icon in the [Sample Table] window
- c. Select [SSM-5000A] for the H/W System Settings
- d. Select icon labeled [Connect] located on the top row of the window
- e. Right click on the number 1 in the Sample Table window and select the [Insert Sample] tab
- f. Select [Calibration curve] parameter and search in the Thawspace (T:) Drive for the folder labeled [SSM-5000A_CalCurve].
- g. Depending on which type of analysis will be run you will choose the file "TC_CalCurve_SSM5000-A" for Total Carbon or the "IC_CalCurve_SSM5000-A" for Inorganic Carbon.
- h. Select [Next], then specify your [Default Sample Name] (e.g., Bob-Shales) and specify your [Default Sample ID] (e.g., LS_1200)
- i. Select [Next], then assure the units are in mg/L and leave the [Expected Conc. Range] as is, this number is negligible.
- j. Select [Next] and assure your integration time is maxed out at 20:00 min, then select [Finish].

Sample Boat

There are two distinct Tupperware boxes with sample boats depending on which method is used.

- a. When using the TC method, use the box labeled "Heat Treated Sample Boats".
- b. When using the IC method, use the box labeled "Acid Treated Sample Boats".
 - i. Use tweezers to grab a clean sample boat from its respective box and place it on the scale.
 - ii. Once the scale has balanced out and a right directional arrow appears on the screen, press the [O/T] button to tare the scale.

- iii. Carefully use the scoopula to scoop a small amount of your sample into the boat. (ideal weight 30-70 mg)
- iv. Once the scale has balanced out, record the weight in mg. This value is used to calculate the concentration of carbon.

Collecting TC

- a. Return to the [Sample Table] and click on row number 1 where you inserted your first sample and make sure it is highlighted.
- b. Select the [Start] icon located to the left on the second row of the [Sample Table Editor] window.
- c. To run your first sample you will be required to name your Sample Table in the Thawspace (T:) Drive (e.g., Bob_Shales_2017_05_01).
- d. Next, you will be prompted to enter the weight (mg) of your sample obtained from the balance. DO NOT PRESS START.
- e. Carefully open the TC chamber by turning the blue knob counter clockwise and slide the cover over to the right.
- f. Place the boat on the metal sample boat holder, make sure it is aligned so that it fits securely in the boat holder.
- g. Slid the cover back over the chamber and make sure it is tightened by rotating the blue knob in the clockwise direction.
- h. Return to the Enter Sample Amount screen and once the weight is input select [Start].
- i. If all background conditions are met, a green [Ready] icon will appear on the top right window and you will be prompted to [Push the sample boat into the measurement position] which you do by pushing the front blue knob all the way forward.
- j. To view your measurements, click the second blue icon in your sample window, it has an icon of a graph and a syringe.
- k. Once your measurement is complete, you will be prompted to pull the boat back to the cooling position, this is the position located between the [sample change] and [measuring] position on the top panel of the instrument.
- l. Once the boat has cooled sufficiently, you will be prompted to pull the boat back to the preparation position.
- m. Once the sample boat has reached the [sample change] position, a table with your Total Carbon Concentration will appear.
- n. Open the chamber cover by rotating the blue knob counter clockwise and sliding it over to the right. o. *CAUTION* sample boat will still be extremely hot, use the tweezers and carefully pick up the boat and place it on the hot plate.
- p. To run another sample for TC analysis, repeat the previous steps as necessary.

Collecting IC

- a. Return to the [Sample Table] and click on row number 1 where you inserted your first sample and make sure it is highlighted.
- b. Select the [Start] icon located to the left on the second row of the [Sample Table Editor] window.
- c. To run your first sample you will be required to name your Sample Table in the Thawspace (T:) Drive (e.g., Bob_Shales_2017_05_01).
- d. Next, you will be prompted to enter the weight (mg) of your sample obtained from the balance. DO NOT PRESS START.
- e. Carefully open the IC chamber by turning the green knob counter clockwise and slide the cover over to the right.

- f. Place the boat on the metal sample boat holder, make sure it is aligned so that it fits securely in the boat holder.
- g. Slid the cover back over the chamber and make sure it is tightened by rotating the green knob in the clockwise direction.
- h. Return to the Enter Sample Amount screen and once the weight is input select [Start].
- i. If all background conditions are met, a green [Ready] icon will appear on the top right window. Although you will be prompted to [Push the sample boat into the measurement position], *WAIT* First, pull up on the white plastic nozzle attached to the bottle of phosphoric acid and allow it to fully inject 0.4 mL of acid into the sample boat so IC reaction can occur.
- j. Once the acid has fully injected into the sample boat, push the front green knob all the way forward to the measuring position.
- k. To view your measurements, click the second blue icon in your sample window, it has an icon of a graph and a syringe.
- l. Once your measurement is complete, you will be prompted to pull the boat back to the cooling position, this is the position located between the [sample change] and [measuring] position on the top panel of the instrument.
- m. Once the boat has cooled sufficiently, you will be prompted to pull the boat back to the preparation position.
- n. Once the sample boat has reached the [sample change] position, a table with your Inorganic Carbon Concentration will appear.
- o. Open the chamber cover by rotating the green knob counter clockwise and sliding it over to the right. p. *CAUTION* sample boat will still be extremely hot and may have residual phosphoric acid, use the tweezers and carefully pick up the boat and place it in the beaker with yellow tape labeled Dilute Phosphoric Acid.
- q. To run another sample for IC analysis, repeat the previous steps as necessary.

Saving Results

- a. Once all TC and IC sample analysis has been completed you can compile a comprehensive report of all your data to save.
- b. Select the [File] tab in the top menu bar, scroll down and select [Print] and scroll to the right and select [Sample Report-All]
- c. Ensure that the printer is set to [Microsoft XPS Document Writer] and click [OK]
- d. Save your file to the Thawspace (T:) Drive so that you can email yourself the results for use the UTA Box sync cloud service.
- e. Once all analyses are saved it would behoove you to open up an MS Excel spreadsheet and create a table of all of your samples with TC in one column and IC in another to easily subtract them to get the sample TOC values. Remember: $TOC = TC - IC$

References

- Allen, R. 2000. Stratigraphy, Mountain Building and Complex Geological Structures of the Ardmore Basin. *Oklahoma City Geological Society. Shale Shaker*, 51(1): 11-21.
- Anovitz, L.M., D.R. Cole. 2015. Characterization and Analysis of Porosity and Pore Structures. *Reviews in Mineralogy and Geochemistry*, 80: 61-164.
- Ballotpedia. 2015. *Oil and Gas Production in Oklahoma*. Released on November 5th, 2015. Available at https://ballotpedia.org/Oil_and_gas_production_in_Oklahoma. Accessed 20 November 2016.
- Barber, T., C. Flaum, D. Ellis, L. Jacobson, M. Smith. 1991. Vertical Resolution of Well Logs: Recent Developments. *Oilfield Review*, 24-28.
- Bennion, D.B., F.B. Thomas, R.F. Bietz. 1996. Determination of initial fluid saturation – a key factor in by-passed pay determination. *Hycal Energy Research Laboratories Ltd*, 1-9.
- Blackford, M.A. 2007. Electrostratigraphy, Thickness and Petro-physical Evaluation of the Woodford Shale, Arkoma Basin, Oklahoma [M.S. Thesis]: Stillwater, Oklahoma State University, 64 p.
- Boyd, D.T. 2012. Oklahoma 2011 Drilling Highlights. *Shale Shaker, The Journal of the Oklahoma City Geological Society*, 62(5): 378-393.
- Burch, G. 2016. Woodford Stratigraphy, personal communication.
- Cardott, B.J. 2013. Woodford Shale: From Hydrocarbon Source Rock to Reservoir. Presentation at the AAPG Woodford Shale Forum held in Oklahoma City, Oklahoma, USA, 11 April, 2013.
- Carvajal-Ortiz, H, T. Gentzis. 2015. Critical Considerations when assessing hydrocarbon plays using Rock-Eval pyrolysis and organic petrology data: Data quality revisited. *International Journal of Coal Geology*, 125; 113-122.

- Chipera, S.J., and D.L. Bish. 2013. Fitting full x-ray diffraction patterns for quantitative analysis: a method for readily quantifying crystalline and disordered phases. *Advances in Materials Physics and Chemistry*, 3: 47-53.
- Chipera, S.J., and D.L. Bish. 2002. A full pattern quantitative analysis program for X-ray powder diffraction using measured and calculated patterns. *Journal of Applied Crystallography*, 35: 744-749.
- Comer, J.B. 2008. Distribution and Source Rock Characteristics of Woodford Shale and Age-Equivalent Strata. Poster Panel Presented at 2008 AAPG Annual Convention held in San Antonio, Texas, USA April 2008.
- Comer, J.B. 2008. Reservoir Characteristics and Production Potential of the Woodford Shale. *Indiana Geological Society*: 1-11.
- Ding, D.Y., Y.S. Wu, N. Farah, C. Wong, and B. Bourbiaux. 2014. Numerical Simulation of Low Permeability Unconventional Gas Reservoirs. *Society of Petroleum Engineers*. SPE 167711, 1-30.
- DrillingInfo. 2010. Continental Provides Good Maps of the Anadarko Basin. <http://info.drillinginfo.com/continental-provides-good-maps-of-the-anadarko-basin/>. Accessed 20 November 2016.
- EIA (Energy Information Administration). 2015. *Annual Oklahoma Crude Oil Proved Reserves*. Available at https://www.eia.gov/opendata/qb.php?category=294161&sdid=PET.RCRR01SO K_1.A. Accessed 2 April 2017.
- EIA (Energy Information Administration). 2016. *Lower 48 States Shale Plays*. Updated on June 30, 2016. Available at https://www.eia.gov/maps/images/shale_gas_lower48.pdf. Accessed April 2, 2017.

- EIA (Energy Information Administration). 2016. *Woodford Shale Play Ardmore Basin*.
Updated on June 1, 2011. Available at
https://www.eia.gov/oil_gas/rpd/shaleusa8.pdf. Accessed February 10, 2017.
- Ewing, R.P., and R. Horton. 2002. Diffusion in sparsely connected pore spaces:
Temporal and spatial scaling. *Water Resources Research*, 38: 10.
- Fertl, W.H., and G.V. Chilingarian. 1990. Hydrocarbon Resource Evaluation in the
Woodford Shale Using Well Logs. *Journal of Petroleum Science and
Engineering*, 4 (4): 347-357.
- Gao, Z., and Q.H. Hu. 2012. Using spontaneous water imbibition to measure the effective
permeability of building materials. *Special Topics and Reviews in Porous Media –
An International Journal*, 3 (3): 209-213.
- Gao, Z., and Q.H. Hu. 2013. Estimating permeability using median pore-throat radius
obtained from mercury intrusion porosimetry. *Journal of Geophysics and
Engineering*, 10: 1-7.
- Gomari, S.R., N. Joseph. 2016. Study of the effect of clay particles on low salinity water
injection in sandstone reservoirs. *Energies*, 10 (322): 1-12.
- Granath, J. 1989. Structural Evolution of the Ardmore Basin, Oklahoma: Progressive
Deformation in the Foreland of the Ouachita Collision. *Tectonics*, 8 (5): 1015-
1036.
- Gupta, N., C.S. Rai, C.H. Sondergeld. Petrophysical Characterization of the Woodford
Shale. *Petrophysics*, 54 (4): 368-382.
- Hager, J. 1998. Steam drying of porous media. PhD thesis, Department of Chemical
Engineering, Lund Univ., Sweden.
- Handwerger, D.A., D. Willberg, M. Pagels, B. Rowland, J.F. Keller. 2012. Reconciling
retort versus dean stark measurements in tight shales, SPE 159976 1-13.

- Harding, T.P. 1974. Petroleum Traps Associated with Wrench Faults. *The American Association of Petroleum Geologists Bulletin*. 58 (7): 1290 – 1304.
- Hu, Q.H., P. Persoff, and J.S.Y. Wang. 2001 Laboratory measurement of water imbibition into low-permeability welded tuff. *Journal of Hydrology*, 242: 64-78.
- Hu, Q.H., R.P. Ewing, and S. Dultz. 2012. Low pore connectivity in natural rock, *Journal of Contaminant Hydrology*, 128: 76-83.
- Hu, Q.H., and R.P. Ewing. 2014. Integrated experimental and modeling approaches to studying the fracture-matrix interaction in gas recovery from Barnett Shale, Final Report, Research Partnership to Secure Energy for America (RPSEA), National Energy Technology Laboratory, Department of Energy, 91p.
- Hu, Q.H., and R. Ewing, and H.D. Rowe. 2015. Low nanopore connectivity limits gas production in Barnett formation [J]. *Journal of Geophysical Research: Solid Earth*, 2015, 120(12): 8073-8087.
- Hughes, J.D. 2015. Revisiting the U.S. Department of Energy Play-By-Play Forecasts Through 2040 from Annual Energy Outlook 2015. *Post Carbon Institute*.
- Jarvie, D.M., 2008. Geochemical Characteristics of the Devonian Woodford Shale. Presentation at Oklahoma Gas Shales meeting held in Oklahoma City, Oklahoma, USA, 22 October 2008.
- Jarvie, D.M., 2012. Shale Resource Systems for Oil and Gas: Part 2 – Shale-oil Resource Systems. *American Association of Petroleum Geologist Memoir 97*, 89–119.
- Jarvie, D., B. Claxton, B. Henk, and J. Breyer. 2001. Oil and Shale Gas from Barnett Shale, Ft. Worth Basin, Texas. Presentation at the AAPG National Convention Denver, CO, USA, 3-6 June, 2001.

- Johannes, I., K. Kruusement, and R. Veski. 2006. Evaluation of oil potential and pyrolysis kinetics of renewable fuel and shale samples by Rock-Eval analyzer. *Journal of Analytical and Applied Pyrolysis*: 1-8.
- Katz, A., and A. Thompson. 1986. A quantitative prediction of permeability in porous rock. *Physical Review B*, 34: 8179-8181.
- Katz, A., and A. Thompson. 1987. Prediction of rock electrical conductivity from mercury injection measurement. *Journal of Geophysical Research: Solid Earth*, 92 (B1): 599-607.
- Kilic, D., and B. Tapp. 2014. Structural analysis of the Eola – Robberson Field using balanced cross sections, Garvin County, Oklahoma. *Oklahoma Geological Survey Guidebook 38*: 341-356.
- King, R.R., D. Jarvie, D. Cannon, T. R. Smith, D. Weldon, and A. Maende. 2015. Addressing the Caveats of Source Rock Pyrolysis in the Unconventional World: Modified Methods and Interpretative Ideas. Presentation at the Unconventional Resources Technology Conference, San Antonio, Texas, USA, 20-22 July 2015.
- Kloubek, J. 1981. Hysteresis in porosimetry. *Powder Technology*. 29; 63-73.
- Kuila, U., and M. Prasas. 2012. Specific surface area and pore-size distribution in clays and shales. *Geophysical Prospecting*. 61 (2): 341-362.
- Lohr, S.C, E.T. Baruch, P.A. Hall, M.J. Kennedy. 2015. Is organic pore development in gas shales influenced by the primary porosity and structure of thermally immature organic matter? *Organic Geochemistry* 87: 199-132.
- Mazaheri, A., H. Memarian, B. Tokhmechi, and B.N. Araabi. 2015. Developing fracture measure as an index of fracture impact on well-logs. *Energy Exploration & Exploitation* 33(4): 555-574.

- McCullough, B.J., and R.M. Slatt. 2015. Paleotopographic Control on the Variability of Woodford Shale across the Southern Cherokee Platform Area of Central Oklahoma: a Mechanism for Increased Preservation-Potential of Organic Content. Adapted from oral presentation given at AAPG Southwest Section annual convention, Wichita Falls, TX, USA, April 13, 2015.
- Morow, N. R., and X. Xie. 2001. Oil recovery by spontaneous imbibition from weakly water-wet rocks. *Petrophysics*. 42(04): 313-322.
- Northcutt, A.R., and J.A. Campbell. 1995. Geologic Provinces of Oklahoma. Compiled for the Oklahoma Geological Society.
- Party, M.J., R.A. Wipf, J.M. Byl, J. Lawton, and J.M. Hill. 2008. Woodford Shale, Ardmore Basin, Oklahoma: A developing Shale Play. Oklahoma Geological Society Archives.
- Passey, Q.R., K.M. Bohacs, W.L. Esch, R. Klimentidis, and S. Sinha. 2010. From oil-prone source rock to gas-producing shale reservoir – geologic and petro-physical characterization of unconventional shale-gas reservoirs. Presentation at the CPS/SPE International Oil and Gas Conference and Exhibition held in Beijing, China, 8-10 June 2010. SPE 131350.
- Pearson, O.N., and J.J. Miller. 2014. Chapter 11 Tectonic and Structural Evolution of the Anadarko Basin and Structural Interpretation and Modeling of a Composite Regional 2D Seismic Line. U.S. Geological Survey Digital Data Series DDs-69-EE.
- Puckette, J., D.R. Boardman, and W.L. Watney. 2013. Woodford Shale: Correlating Rock Properties in Outcrop and Core with Wireline Log Characteristics. Adapted from oral presentation at Tulsa Geological Society Luncheon meeting, Tulsa, OK, USA, 24 September, 2013.

- Rezaee, R. 2015. *Fundamentals of Gas Shale Reservoirs*: John Wiley & Sons.
- Slatt, R. 2013. *Sequence Stratigraphy of the Woodford Shale and Application to Drilling and Production*. Adapted from oral presentation given at AAPG Woodford Shale Forum, Oklahoma City, OK, USA, 11 April, 2013.
- Smithson, T. 2012. How porosity is measured. *Oilfield Review*, 24 (03): 63-64.
- Sondergeld, C.H., K.E. Newsham, J.T. Comisky, M.C. Rice, and C.S. Rai. 2010 *Petro-physical Considerations in Evaluating and Producing Shale Gas Resources*. Presentation given at the SPE Unconventional Gas Conference held in Pittsburgh, Pennsylvania, USA, 23-25 February, 2010.
- Suneson, N. 1996. *The Geology of the Ardmore Basin in the Lake Murray State Park Area, Oklahoma: An Introduction and Field Trip*. Presentation at the Spring Field Meeting of the Oklahoma Academy of Science held in Ardmore, Oklahoma, USA. 26-28 April, 1996.
- Wang, S., F. Javadpour, and Q.H. Feng. 2016. Confinement correction to mercury intrusion capillary pressure of shale nanopores. *Scientific Reports*, 6: 20160, doi:10.1038/srep20160.
- Washburn, E.W. 1921. Note on a method of determining the distribution of pore sizes in a porous materials. *Proceedings of the National Academy of Sciences, U.S.A.*, 7; 115-116.
- Webb, P.A. 2001. An introduction to the physical characterization of materials by mercury intrusion porosimetry with emphasis on reduction and presentation of experimental data. *Micromeritics Instrument Corporation*.

Biographical Information

Benjamin Elliott Ryan is from Fort Worth, Texas and graduated from Fort Worth Country Day High School before attending Texas A&M University in College Station, Texas where he received a Bachelor of Science Degree in Geology. Shortly after graduating from Texas A&M he attended the University of Texas at Arlington where he received a Master of Science Degree in Petroleum Geology. Throughout his undergraduate and graduate studies he worked in the petroleum industry and plans to continue to pursue a career as a petroleum geologist.